BAND GAP STRUCTURE OF TWO DIMENSIONAL ACOUSTIC METAMATERIALS WITH COATED DOUBLE HYBRID LATTICE

by

Yanbo He

B.S. in Thermal Power and Energy Engineering, Harbin Engineering University, 2014

Submitted to the Graduate Faculty of

Swanson School of Engineering in partial fulfillment

of the requirements for the degree of

Master of Science in Mechanical Engineering

University of Pittsburgh

2015

UNIVERSITY OF PITTSBURGH

SWANSON SCHOOL OF ENGINEERING

This thesis was presented
by

Yanbo He

It was defended on

November 16, 2015

and approved by

Jeffrey S. Vipperman, Ph.D, Professor,

Department of Mechanical Engineering and Materials Science

William W. Clark, Ph.D, Professor,

Department of Mechanical Engineering and Materials Science

Albert To, Ph.D, Associate Professor,

Department of Mechanical Engineering and Materials Science

Thesis Advisor: Jeffrey S. Vipperman, PhD, Professor,

Department of Mechanical Engineering and Materials Science

BAND GAP STRUCTURE OF TWO DIMENSIONAL ACOUSTIC METAMATERIALS WITH COATED DOUBLE HYBRID LATTICE

Yanbo He, M.S.

University of Pittsburgh, 2015

Acoustic metamaterials (phononic crystals) have received much recent attention. Over time, several efforts were proposed to improve the structure in order to enlarge the band gap, lower the band gap frequency, and/or generate greater attenuation of vibration. In this document, a novel two dimensional acoustic metamaterial with Coated Double Hybrid Lattice (CDHL) is proposed. The structure makes use of both the Bragg Scattering Theorem and the Local Resonance Theorem. In the simulation, both a lower frequency band gap and a higher frequency band gap are obtained. According to the modal analysis and phase spectrum analysis, it is proved that the lower frequency band gap is due to local resonance between the double lead cores and the rubber coating. At the same time, the higher frequency band gap is generated as a result of the interaction of Bragg scattering and local resonance effect. The variation in maximum vibration attenuation with respect to the position of the double central lead core is also investigated. Excellent vibration attenuation is demonstrated using the proposed method. Later on, experiments are carried out both to validate the simulation and to prove the effectiveness of the proposed structure. The output signal is picked up approximately in the middle of the structure

and the results have coincides with the simulation quite well. At the end of this document, several outlooks are stated.

TABLE OF CONTENTS

LIST OF TABLES

LIST OF FIGURES

PREFACE

First of all, I would like to thank Dr. Vipperman who made this research possible. During the one and a half years, I really enjoyed the meetings that we had each time and the moments that we worked together.

Special thanks to doctoral student Qi Li for providing the comments and advice. We always have constructive discussions throughout the entire project. During the structure manufacturing, Mr. J. Andrew Holmes and Mr. Thorin Tobiassen always answered questions and helped me with the operations. I greatly appreciate it. During the experimental study, Mr. Christopher Michael Dumm helped me a lot with the original attempts. I learned a lot from him and I really enjoyed the time that we worked together. In the meantime, I am also appreciative of the suggestions provided by doctoral students Timothy S. Ryan and Brandon Robert Saltsman. Furthermore, I would also like to thank Dr. Sung Kwon Cho and doctoral student Jian Feng for the help with MSA-400 equipment, without whom I will never finish my experiments.

Finally, many thanks to Swanson School of Engineering for all the support. I always enjoy the time that I spend here.

1.0 INTRODUCTION

Over the past decades, there has been growing interests in exploring new periodic materials/structures which exhibit band gaps, called acoustic metamaterials (phononic crystals)[1]. Research of acoustic metamaterials traces back to the year 1992, when Sigalas et al. theoretically proved the existence of a band gap structure in periodic structures[2]. Later on, Kushwaha et al. demonstrated the concepts of phononic crystals for the first time[3]. In 1995, Martinez-Sala et al. carried out an experiment on sculptures by the Juan March Fondation. They observed that during a certain range of sound frequencies, the sound is clearly attenuated so that for the first time, a band gap was observed and investigated[4]. From then on, the field of acoustic metamaterials have attracted attention from all over the world. As a new type of material/structure, it possesses profound theoretical values and these have led to a great variety of applications.

Figure 1.1 Kinematic sculpture by Eusebio Sempere[4]

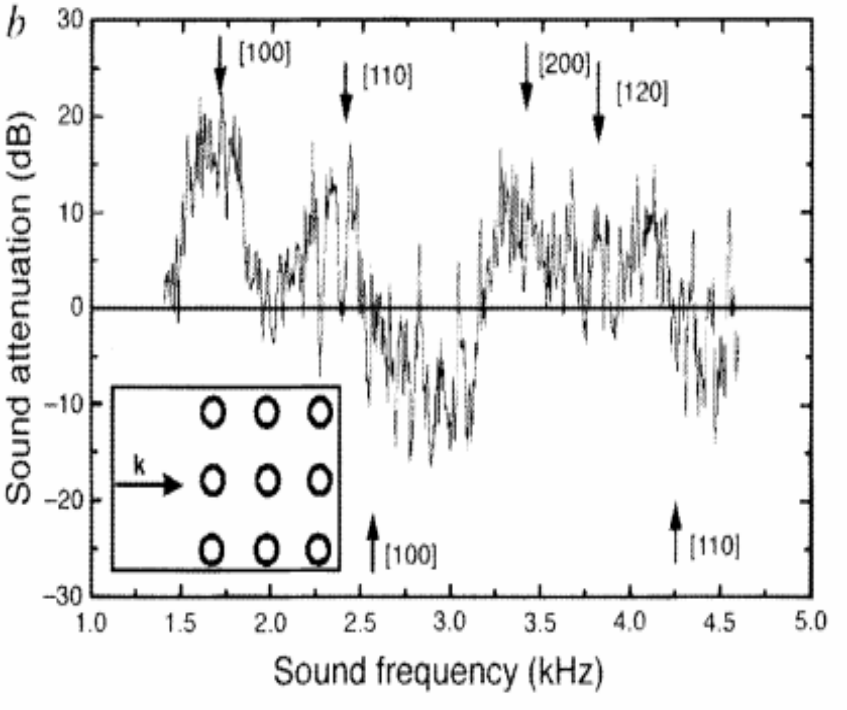

Figure 1.2 Sound attenuation results as a function of the sound frequency[4]

Of all these special characteristics, one of the most attractive ones is the band gap generated, that is, in specific frequency ranges, the propagation of elastic waves is prohibited. By making use of the band gap that has been generated, people discovered that it was a promising candidate for applications such as the vibration attenuation[5], wave guiding[6], acoustic filters[7], acoustic sensors and actuators[8]. Based on these principles, recent advancements have focused on enlarging the band gap, lowering the band gap frequency and obtaining greater vibration/acoustic attenuation. Mainly, there are two theorems that are responsible for the generation of a band gap. In either the ultrasonic or supersonic frequency range, where the vibration wavelength is approximately at the same order as the structure, the gap generated is mainly due to Bragg scattering whereas in the audible frequency range, where the vibration wavelength is much greater than the structure, the gap generated is mainly due to local resonance.

1.1 OVERVIEW OF BAND GAP GENERATION THEOREM

1.1.1 Bragg scattering derived band gap

The gap created due to Bragg scattering is actually a kind of traditional band gap that was found a couple of decades ago[9]. It results from the scattering of acoustic or elastic waves in a fashion analogous to Bragg scattering of X-rays by periodic structures. Since this kind of band gap is usually generated at a frequency which lies in the ultrasonic or supersonic range, where the wavelength is a lot greater than the lattice constant, it will be affected by the material parameters of the scatterers[10]. For example, by investigating the effects of material parameters on the two dimensional and three dimensional solid phononic crystals, Zhou et al. [11]and Ma et al.[12]

concluded that the density ratio, the longitudinal and transverse velocity ratio of scatterers and background matrix, as well as the filling fraction of the lattice would have a clear impact on both the position and width of the band gap. Also, greater disparities of these parameters, will yield wider and lower the band gaps. On the other hand, the geometrical characteristics of the scatterers also have a clear impact. Therefore, people have additionally investigated how the geometries of the scatterers will affect the band gap structure. Some typical shapes of scatterers are circles[13], squares[14], triangles[15], hexagons[16] etc. Some typical shapes of the lattice are also investigated such as squares[17], rectangles[18], FCC[19].s

Based on these results, further refinement of the band gap based on basic shapes of scatterers was carried out. One of the valid proposals was to rotate the scatterers. Du et al. have investigated variations of out plane wave band gaps corresponding to the varied rotation angles of scatterers[20]. They show the out-of-plane wave band gap will first be narrowed and then be enlarged with the increase of the rotation angle.

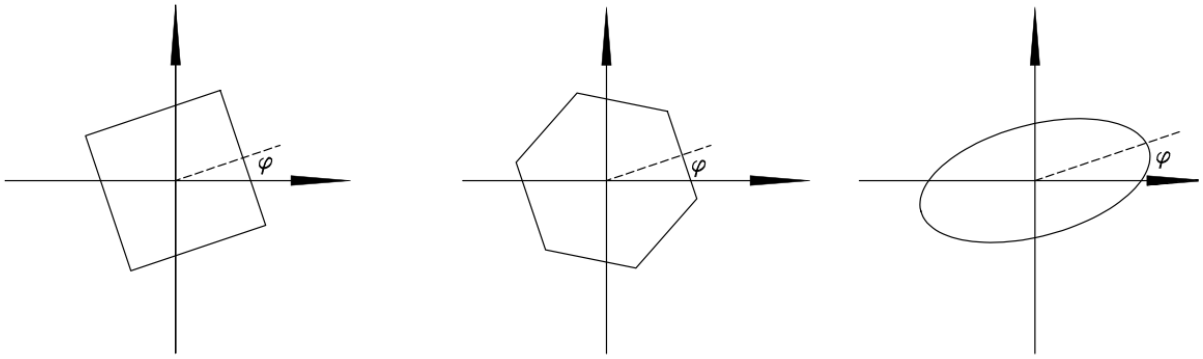

Figure 1.3 Schematic of various shapes of scatterers after rotation[20]

Apart from rotating the scatterers, rearranging the scatterers inside the lattice is also shown to be effective. As shown in Figure 1.4, Yao et al. added an extra square scatterer into the center of the lattice[21].

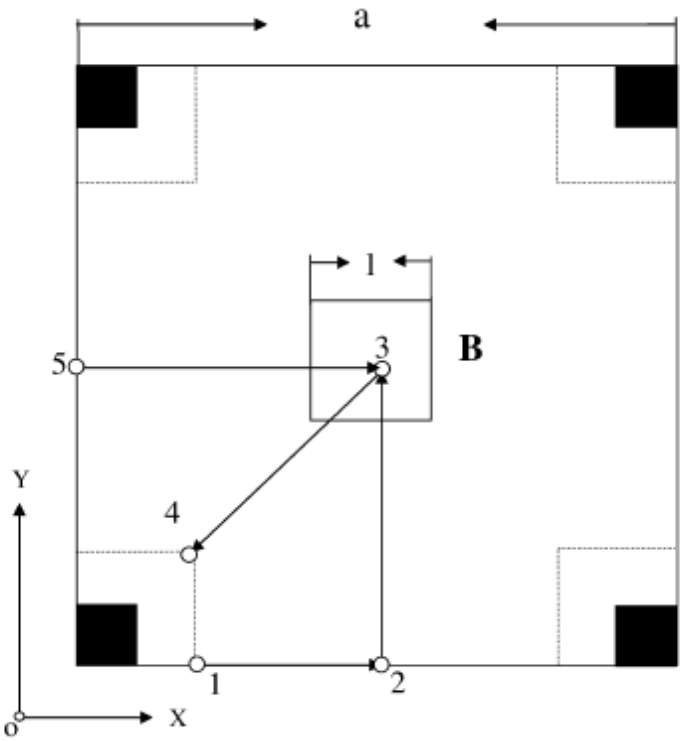

Figure 1.4 Schematic of hybrid lattice with extra square scatterers added in the center[21]

By varying the position of the central square scatterers and changing the dimension of the scatterers at all four corners, the band gap obtained is greatly enlarged. Also, in the most recent literature, Aravantinos et al. have numerically examined a novel large scale structure in order to isolate the seismic vibration[22].

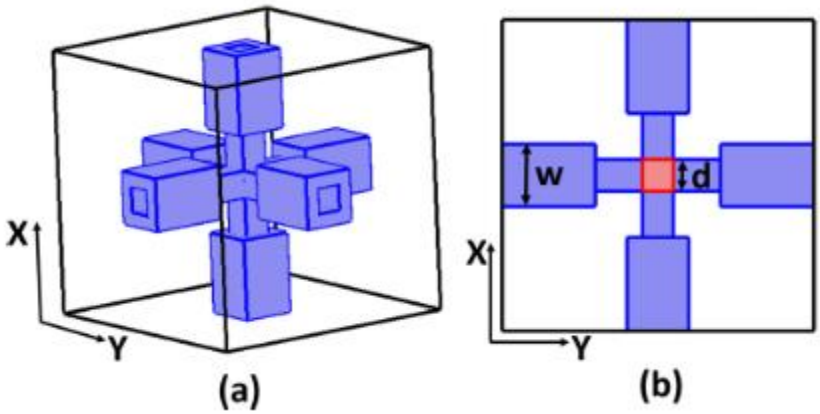

Figure 1.5 Computation structure of a unit cell (a) and (b) the X-Y plane at the center of the computation structure[22]

By varying the dimension of the layer-by-layer structure, a varied band gap is obtained and studied. However, despite the fact that all the above works have successfully come up with Bragg scattering derived band gaps, there is still a limitation, that is, the frequency areas of the band gaps obtained are always placed in either the ultrasonic or the supersonic frequency range. As a result, if a Bragg scattering derived audible frequency band gap is to be obtained, people will have to replicate Aravantinos' work and fabricate a structure with the dimension of approximately the same as the wavelength of the audible frequency vibration that is to be attenuated. Since that dimension is usually on the order of meters, it will cause a lot of incovenience.. Therefore, a local resonance derived band gap is being considered.

1.1.2 Local resonance derived band gap

To overcome the previously mentioned weakness, Liu et al. has come up with a local resonant band gap[23]. By coating the lead core with softer rubber, a local resonance is generated between

the lead and the rubber which opens a sonic band gap. The schematic of the structure is shown in Figure 1.6.

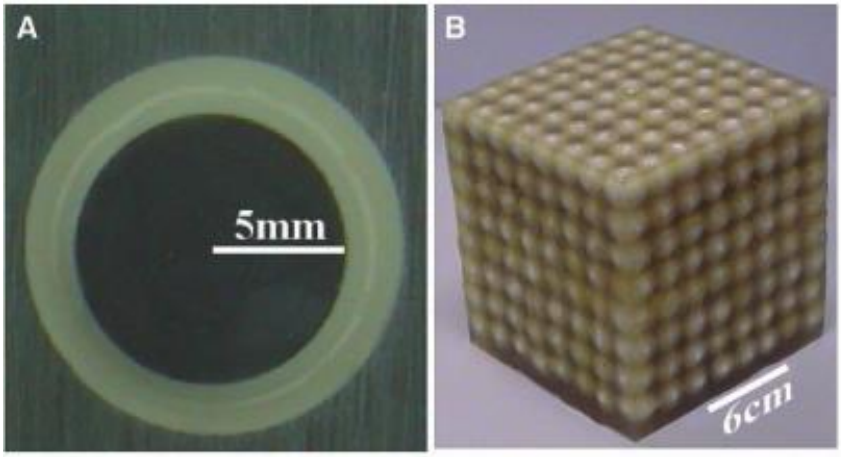

Figure 1.6 Schematic of coated lead sphere[23]

In this case, the exhibited band gap with lattice constants is two orders of magnitude smaller than that at the Bragg frequency. Therefore, the band gap would present at a much lower frequency than the Bragg Scattering Band Gap. Interest in this result has spurred additional research over the past decades. Different kinds of resonators have come into existence. For example, Li et al. have come up with multilayer-split-tube resonators and have formed a Helmholtz resonant phononic crystal[24]. Hsu et al. fabricated an array of stepped resonators in a thin slab[25]. A low-frequency gap within the audible regime has been demonstrated. Larabi et al., presented a multilayer cylindrical structure. By introducing the inclusions of all the shells, they have broken the original gaps into smaller pieces that collectively form wider gaps[26]. Meanwhile, by investigating pattern transformation of deformable materials, Bertoldi et al. related the width

and position of the band gap to the stress applied. Therefore, they have successfully controlled both the position and the width of the band gap by applying external forces[27-28].

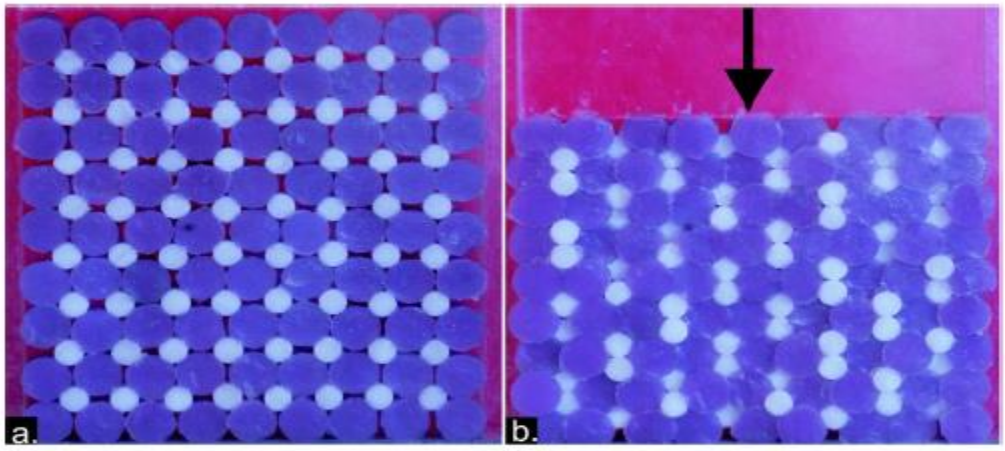

Figure 1.7 Deformation of materials under external forces[27]

1.1.3 Summary of Bragg scattering derived gap and local resonance derived gap

Besides changing the band gap position stated before, there is also the ability to change gap width. For a higher frequency band gap, it is generated by wave scattering. As long as the two waves are of a similar wavelength and that wavelength is about the same order as the lattice constant. Under some specific conditions, they would interact with each other and open a band gap. However, for a lower frequency band gap, it is formed as a result of the local resonance between a hard core and a soft coating. It usually appears at a frequency which corresponds to a specific discretized eigenmode. Hence, it is usually the case that the Bragg scattering derived band gap is wider than the obtained local resonance derived gap[29].

Therefore, theoretically speaking, fabricating a structure that can make use of both the theorems will permit us to modify the band gaps at both low band gap and high at the same time. From a practical standpoint, fabricating a structure that can generate band gaps by making use of these two theorems simultaneously will permit the modification of band gaps at both low (audio-range) and high (ultrasonic range) at the same time. Furthermore, those structures will have potential applications in some areas where there are special vibration attenuation requirements like ultrasonic motors, which are actuated at ultrasonic frequencies, with gross motion at sonic frequencies.

1.1.4 Combination of Bragg scattering derived gap and local resonance derived gap

Concerning the previously mentioned potential application, this document is intended to demonstrate a novel structure that would combine Bragg scattering derived gaps and Local resonance derived gaps. This novel structure is based on a basic work in which by coating the circular scatterers with a softer material and extending the testing frequency range to 120 kHz, Xu et al. has demonstrated the coexistence of a Local resonant and a Bragg scattering band gap[30]. Their structure along with the displacement field is illustrated in Figure 1.8.

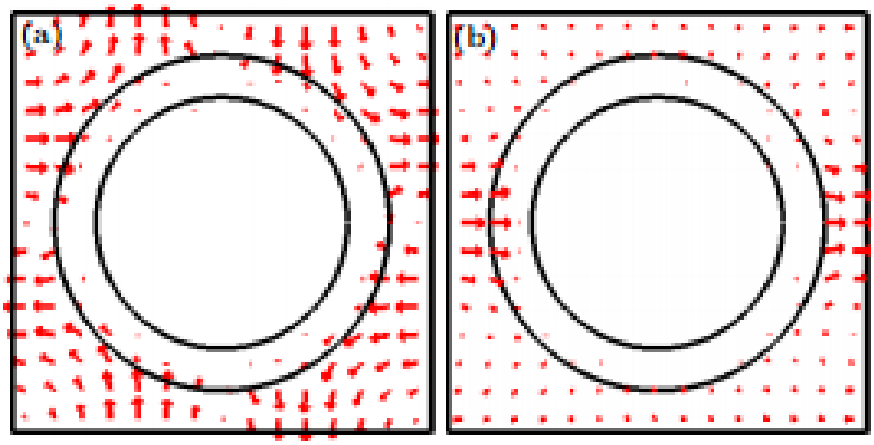

Figure 1.8 Displacement vector field of Xu's structure[30]

By expanding waves along the first irreducible Brillouin zone, a band structure is obtained in Figure 1.9 where both the high frequency and low frequency band gap are obtained in the dark zone. The high frequency band gap is due to Bragg scattering of the plane wave whereas the low frequency band gap is due to local resonance between the steel core and the rubber coating.

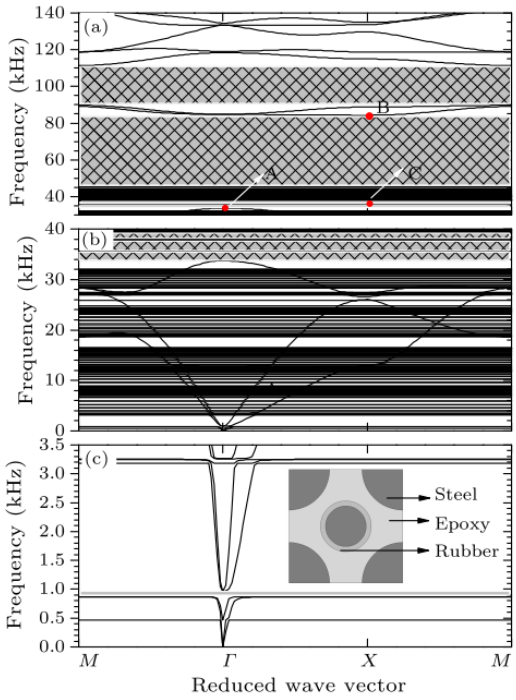

Figure 1.9 Band structures of the composite phononic crystal in (a)40-140 kHz (b)0-40kHz and (c) 0-3.5 kHz The insert in the subplot (c) is the unit cell of the composite phononic crystal[30].

Similarly, Cui et al. put forward a new structure which was composed of a square array of steel tubes with narrow slits[31]. They proved both theoretically and experimentally that traditional Bragg scattering and local resonant band gaps could be produced simultaneously. However, these reports are basic works where only a single shape of the scatterer has been considered. Hence, in this document, a hybrid lattice with different shapes of scatterers combined and central scatterers coated by softer rubber is being considered. In the meantime, apart from a simultaneous appearance of Bragg scattering derived gaps and Local resonance derived gaps, greater vibration attenuation is also expected.

1.2 METHOD OF INVESTIGATION

Over time, to explore the band gap structure of the acoustic metamaterials, researchers have come up with several investigative methods to meet the different requirements of specific problems. Mainly, they are: plane wave expansion method[32] (PWE), transfer matrix method[33] (TM), finite element time domain method[34] (FETD), finite element analysis[35] (FEA), etc.

1.2.1 Transfer Matrix Method (TM)

The transfer matrix method is commonly used to investigate the band gap structure of one dimensional acoustic metamaterials. It is really convenient because, if the field is known at the beginning of a layer, by making use of the continuity of stress and displacement across boundaries from one piezo to another, the field at the end of the layer can be derived from a simple matrix operation. Hence, a stack of layers can then be represented as a system matrix, which is the product of the individual layer matrices. A typical example of this case is the work reported by He et al. where piezoelectric patches were utilized to attenuate the vibration of phononic crystal rods[36].

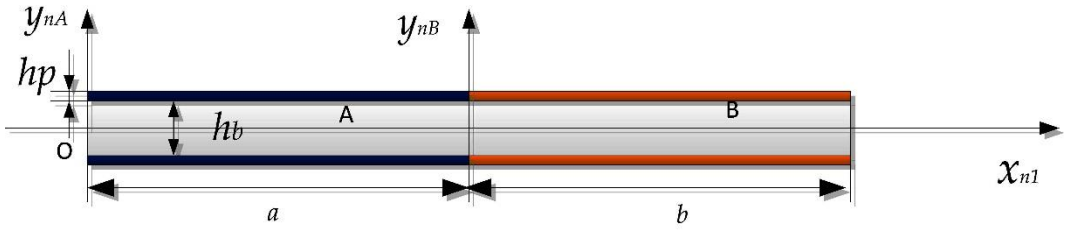

Figure 1.10 Vibration attenuation by hybrid piezoelectric shunted patches[36]

Figure 1.10 illustrates a schematic of a one dimensional rod with piezoelectric patches covered at both sides is illustrated[36]. The one dimensional wave equation is expressed as,

$$\rho \frac{\partial^2 y}{\partial x^2} = \frac{\partial}{\partial x}[E \frac{\partial y}{\partial x}] \quad (1\text{-}1)$$

where ρ and E are the density and the Young's modulus of the rod at the location of x respectively. Suppose that the solution of the equation would have the form of $y = y(x)e^{i\omega t}$ so that the displacement field of the nth part could be expressed as

$$y_n = A_1 \cos(\lambda x_1) + A_2 \sin(\lambda x_2) \quad (1\text{-}2)$$

in which

$$\lambda = \frac{(\rho_b A_b + 2\rho_p A_p)\omega^2}{E_b A_b + 2E_p A_p} \quad (1\text{-}3)$$

where the subscripts b and p represent the rod and piezo patches respectively, and ρ, E and A are the density, the Young's modulus and the area, respectively. Finally, due to stress and displacement continuity at the boundary of each layer, a transfer matrix can be finally fabricated as

$$T = H^{-1}K \quad (1\text{-}4)$$

where H and K are both coefficient matrices. By solving for the eigenvalues of the above matrix, T, a band gap structure can be obtained and studied.

1.2.2 Plane Wave Expansion Method (PWE)

Followed by the transfer matrix method, the plane wave expansion method is also widely used for studying two dimensional acoustic. From the wave propagation point of view, by expanding the elastic wave along the first irreducible Brillouin zone (shown in Fig. 1.11) and forming an eigenvalue problem, a band gap structure can be analyzed.

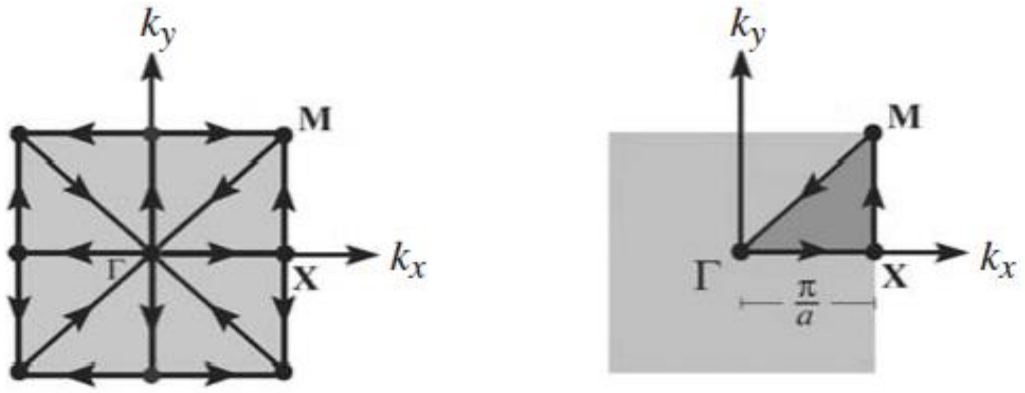

(*a*) **(*b*)**

Figure 1.11 Schematic of (a) the first Brillouin zone and (b) the first irreducible Brillouin zone[37]

Starting from the two dimensional wave equation

$$\rho\ddot{u}_i = \rho f_i + \sum_{j=1}^{3}\left\{\frac{\partial}{\partial x_i}\left(\lambda\frac{\partial u_i}{\partial x_j}\right) + \frac{\partial}{\partial x_j}\left(\mu\frac{\partial u_i}{\partial x_j} + \frac{\partial u_j}{\partial x_i}\right)\right\} \quad (1\text{-}5)$$

where λ and μ are Lamé coefficients, due to periodic characteristic of the structure, the constants in eqn. (1-5) i.e. Lame coefficients and density are all periodic functions with respect to position. Therefore, by defining a reciprocal lattice vector as

$$\boldsymbol{G} = n_x b_x + n_y b_y \quad (1\text{-}6)$$

where n_x and n_y are all integers, according to Bloch theorem of periodicity,

$$\boldsymbol{u}_{k+1}(\boldsymbol{r}, t) = e^{i\boldsymbol{G}\cdot\boldsymbol{r}}\boldsymbol{u}_k(\boldsymbol{r}) \quad (1\text{-}7)$$

by coming up with an eigenvalue problem, a band gap of two dimensional structure can be obtained and studied.

1.2.3 Finite Element Analysis (FEA)

Apart from the above methods, there is also another traditional method which is valid for both one dimensional and two dimensional problem analysis, that is, the finite element analysis

method (FEA). This is the method used throughout the entire document, the procedure of which could be summarized as below.

One will start from the two dimensional wave equation, as illustrated by eqn. (1-5) and discretize the structure under analysis. Then, applying the Bloch periodic condition to the boundaries[38]

$$\boldsymbol{u}_{k+1}(\boldsymbol{r}) = e^{i\boldsymbol{k}\cdot\boldsymbol{r}}\boldsymbol{u}_k(\boldsymbol{r}) \tag{1-8}$$

where *k* is the Bloch wave number which is defined in the first irreducible Bloch zone, one can solve the problem with the unknowns and analyze the results.

1.3 MEASUREMENT OF BAND GAP STRUCTURE

As indicated in the previous sections, this document is intended to both analytically and experimentally study the band gap structure of a novel two dimensional acoustic metamaterials. To explore the vibration attenuation by the proposed structure and to understand the physical mechanism for generation, some terminologies are defined and several parameters are measured.

1.3.1 Terminology

Before the measurement discussion, several terms need to be defined since they will appear throughout the whole document[38].

- Midgap

This is the term used to describe where the band gap exists. The mathematical equation for the midgap can be expressed as

$$m = \frac{(upper\ band + lower\ band)}{2} \quad (1\text{-}9)$$

- Gap width

As is indicated by its name, this is the term used to describe the bandwidth of the gap being generated, which can be expressed as

$$w = upper\ band - lower\ band \quad (1\text{-}10)$$

1.3.2 Transmission

Transmission is defined as a ratio of the transmitted sound power and the incident sound power[38]. The transmission is expressed mathematically as

$$T = 10 * \log\left(\frac{w_t}{w_i}\right) \quad (1\text{-}11)$$

where w_t and w_i are the transmitted sound power and incident sound power respectively. Studying the transmission is very important since it will enable us to visualize the vibration attenuation in the band gap. In the band gap frequency where the elastic wave is prohibited from propagating, the transmission coefficient will significantly decline compared with the ordinary wave propagation case. Therefore, it is a great indicator for the position as well as the width of the band gap that has been generated. Moreover, by looking at the transmission spectrum, one can qualitatively discern the physical mechanism of gap formation.

1.3.3 Modal Analysis

The phase calculation has informed us a way to identify whether or not Bragg scattering happens. To further identify the local resonance effect, one has to carry out modal analysis[40]. The

goal of the modal analysis is to determine natural mode shapes and frequencies of an object or structure during free vibration. The physical interpretation of eigenvalues and eigenvectors which come from solving the system are that they represent frequencies and corresponding mode shapes. Different from picking up an infinite structure, one would only need to take one period of the whole structure. Once a local resonance takes place at specific frequency, an eigenmode will be found. Therefore, this document will identify the local resonance effect by carrying out modal analysis for a single period of structures.

1.3.4 Experimental equipment

The following equipment is needed for measuring the band gap structure of the proposed structure:

- Function generator: AGILENT 33220A

This is used to generate sinewaves of various frequencies. The maximum amplitude of the signal is 20 V.

- Amplifier: Trek Model 2100 HF piezo driver

This is used to amplify the input signal. The signal will be amplified by 50 times after going through the amplifier

- Actuator: D020010 piezo stacks, Kinematic Ceramics Inc.

The actuator is used to generate plane waves. According to our experiments, the resonances of the actuators are at 16 kHz and 20 kHz.

- Sensor: MSA-400, Polytech Inc.

The sensor is used to test the output response. The sensor will have the following features.

- Sampling frequency: 512 kHz

- Sampling time: 32 ms
- NFFt: 6400
- Resolution: 31.25Hz

2.0 ANALYTIC STUDY

From this chapter on, an analytic study is carried out to demonstrate the proposed structure. Also, several efforts were made to prove the effectiveness of the given structure in vibration attenuation. The parameters that will be calculated throughout the chapter have already been stated in the introduction chapter.

2.1 SINGLE COATED LATTICE

Before presenting the proposed structure, a simpler structure was analyzed that was similar to a structure from the literature, with only one coated circular scatterer in the center, as shown in Figure 2.1. The lattice has a side length of a=0.01 m, which is also defined as the lattice constant.

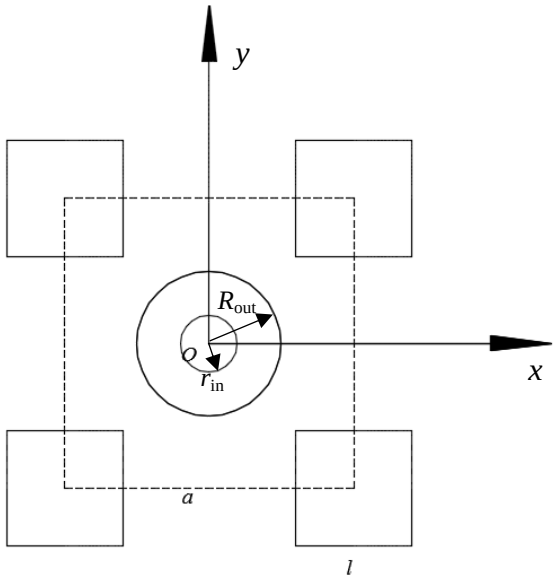

Figure 2.1 Schematic of single coated hybrid lattice

The structure consists of three different materials. The background matrix is made of epoxy. The central core as well as the four square scatterers at the corners are all made of lead. Meanwhile, the central lead core is coated with softer silicone rubber. The related parameters of these materials are stated in Table 2.1. After a considerable amount of simulation with various geometric parameters, the geometric parameters, R_{out}=0.0025 m, r_{in}=0.001 m, l=0.004 m, are finally chosen which present the best balance in width and attenuation in this case.

Table 2.1 Related material parameters

materials	parameters		
	Density ρ (kg/m^3)	Young's Modulus E (GPa)	Poisson's ratio μ
lead	11,400	23.7	0.41
epoxy	1,200	4.1	0.40
rubber	1,000	1×10^{-3}	0.48

Theoretically, what we are looking at is an infinite lattice; that is, it should be infinite in both *x* and *y* directions. A single cell of this lattice is shown in Figure 2.1. However, to simplify the numerical simulation without losing generality, we have chosen 10 periods in the *x* direction and infinite in the *y* direction. The infiniteness is accomplished by setting a Bloch periodicity boundary condition on both the top and bottom boundaries of the structure as shown in Figure 2.2.

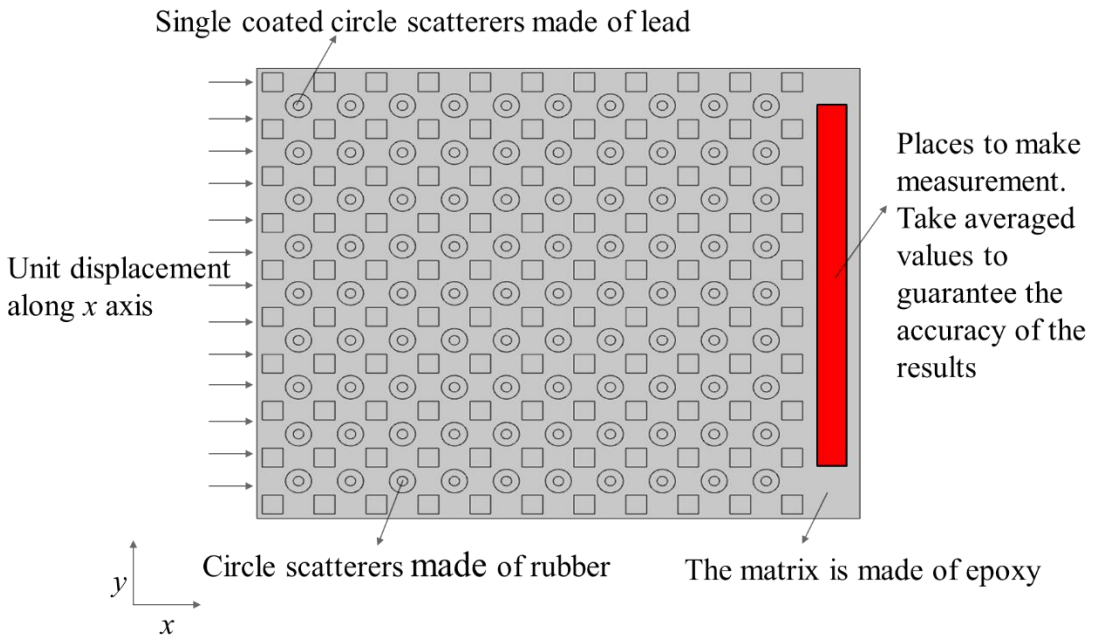

Figure 2.2 Schematic of single coated hybrid acoustic metamaterials

First, as introduced in the first chapter, a unit dynamic displacement is introduced on the left side of the lattice. The displacement along *x* axis is placed as

$$U_x = 1 * e^{-ik \cdot x} \tag{2-1}$$

where *k* is the wavenumber defined as

$$k = \frac{2\pi f}{c} \tag{2-2}$$

with the frequency varied from 0 to 120 kHz. Also, in eqn. (2-1) *x* equals -0.15 in this case. Meanwhile, the equation (2-1) has illustrated that the input is a dynamic displacement with an amplitude of 1 m, which may seem to be odd at first glance. However, it is the transmission that we calculate throughout the documents, and it is the ratio relationship between output and input that we are looking for. Therefore, the exact value of the displacement does not really matter; in other words, we will always obtain the same results when the amplitude of displacement is set to

1 cm, 1 mm, etc. The measurement of the output displacement is taken in the red zone at the right side of the lattice. To improve the accuracy of the results, measurements from five different points in the zone are obtained and then averaged. When the vibrational transmission is calculated for the frequency range from 0 Hz to 120 kHz, the following result is obtained:

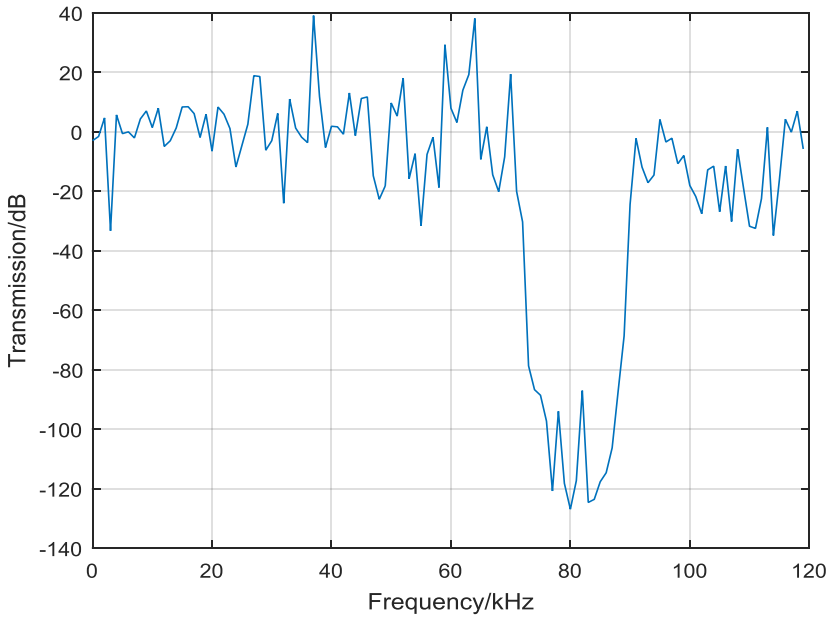

Figure 2.3 Band gap structure of single coated hybrid lattice

It is quite clear from Figure 2.3 that multiple band gaps can be observed across the whole investigated frequency range. These gaps can be divided into two categories depending on their position. First of all, there is a very wide vibration attenuation starting from 70 kHz and ending at 90 kHz. It is a band gap with a gap width of 20 kHz and the maximum simulated vibration attenuation of over 120dB. It is also important to concentrate on another band gap that is situated between 2 kHz and 4 kHz. Indeed, in Figure 2.3, we may find several frequencies where vibration is attenuated. However, the band gaps are expected to appear at 2-4 kHz and 70-90 kHz

for different mechanisms and they are observed in the experimental results. On one hand, the higher frequency band gap is believed to be generated by Bragg scattering since it is wide with great vibration attenuation. In that case, the wavelength of scattered waves in the given frequency range is about the same order as the lattice constant. On the other hand, the generation of the lower frequency band gap should be owing to local resonance since the wavelength of the propagating wave in this range is a lot greater than the lattice constant. Furthermore, the gap width obtained is narrower than that presented by the higher frequency band gap.

In conclusion, the simulation results suggest a 33.3 dB theoretical vibration attenuation could be obtained.

2.2 COATED DOUBLE HYBRID LATTICE (CDHL)

To obtain a greater vibration attenuation in the lower frequency range, we have proposed an alternate physical structure which is referred to as a "Coated Double Hybrid Lattice" (CDHL). Due to the specially designed structure of CDHL, a flexural mode will be introduced which has been observed to enhance the vibration attenuation[39]. The schematic of the whole structure is shown in Figure 2.4, whereas the single lattice is illustrated by Figure 2.5.

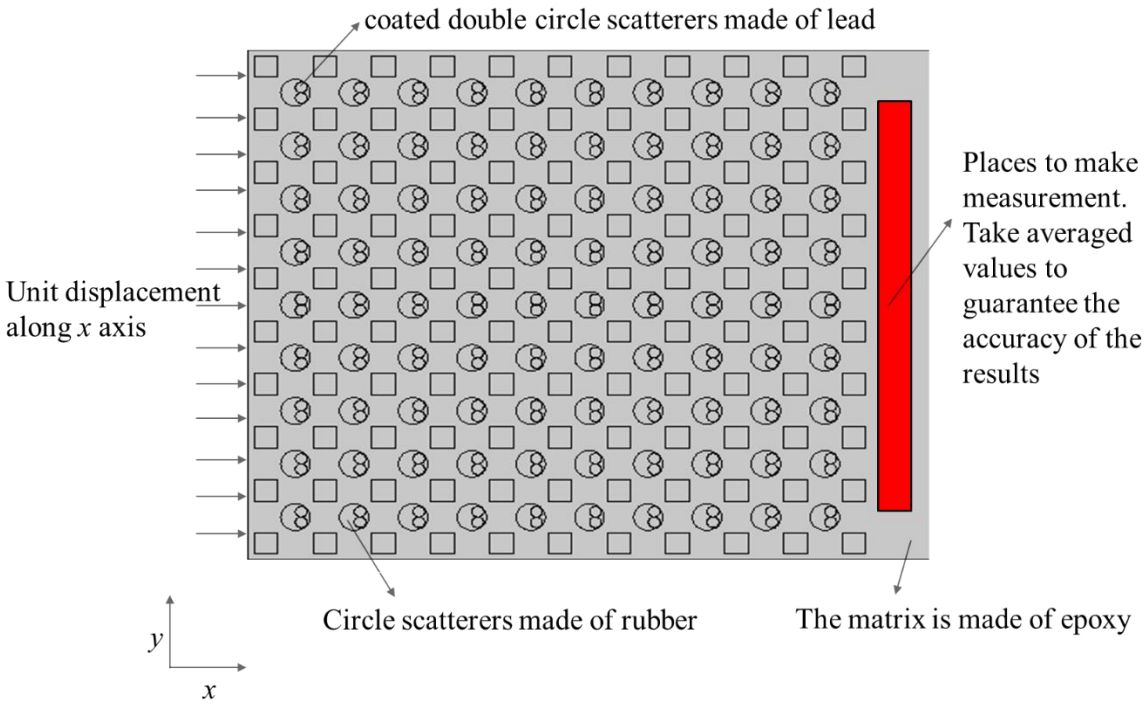

Figure 2.4 Schematic of CDHL

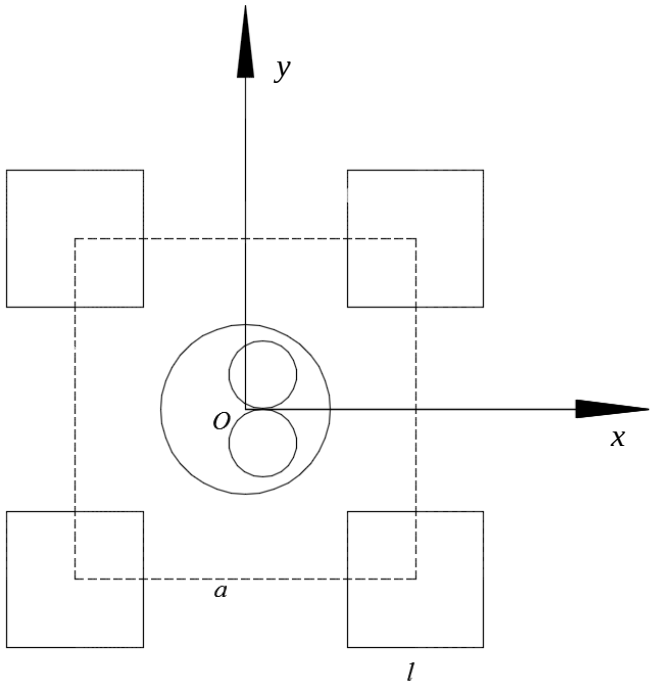

Figure 2.5 Schematic of CDHL with single lattice

The structure is quite similar to the original case, with four square lead scatterers located in the corners and a circular scatterer in the center. But quite differently from original case, the circular scatterer is formed by two small lead scatterers of the same size, which are coated by a large silicon rubber scatterer. The geometry is heuristically optimized to obtain best balance of width and attenuation by running several trials using FEA. Epoxy is still utilized as the matrix. Figure 2.6 shows the transmission for the CDHL, which will be discussed below

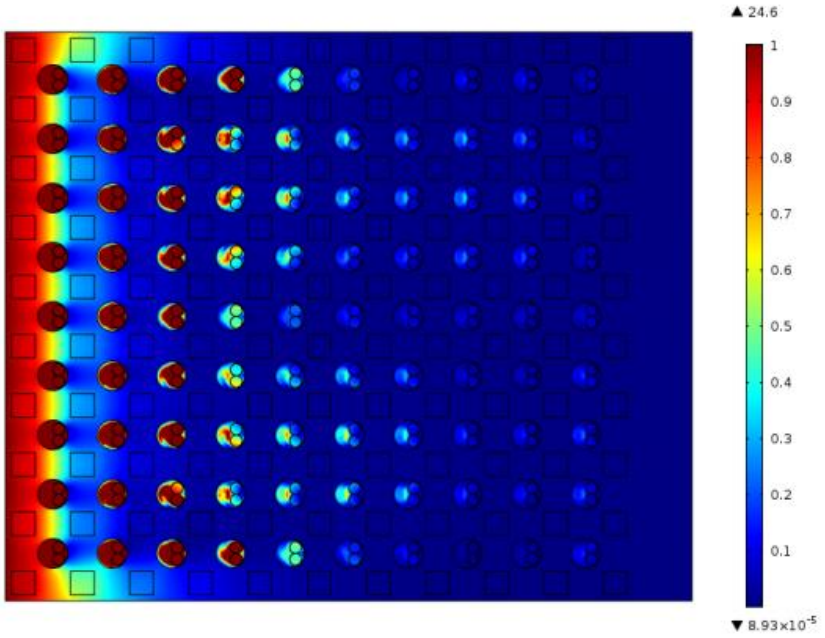

Figure 2.6 Characteristic of wave propagation in lower frequency band gap

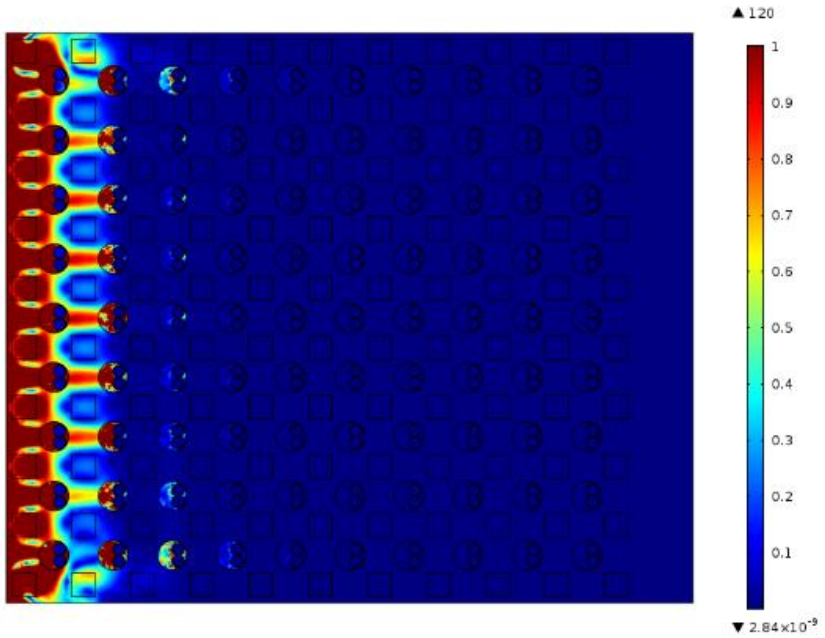

Figure 2.7 Characteristic of wave propagation in higher frequency band gap

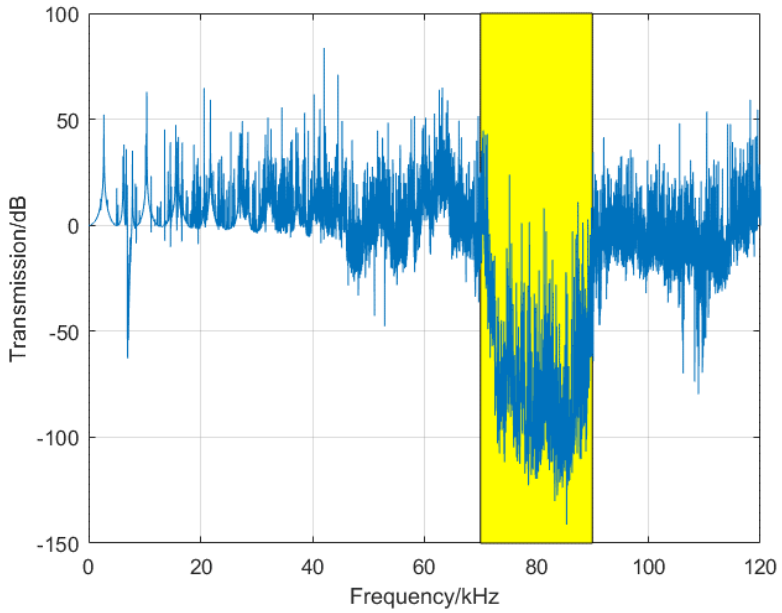

Figure 2.8 Transmission for CDHL

Presented in Figure 2.6 and Figure 2.7 are the detailed characteristics of wave propagation through the structure. The vibration originating from the left is quickly attenuated as

it propagates to the right. In Figure 2.6, it is clear that the circle scatterers are excited. Therefore, it is the case where the wave propagation is attenuated due to the local resonance between the lead cores and rubber coating. However, in Figure 2.7, none of the scatterers are excited and the vibration is attenuated due to the Bragg scattering effect. Due to local resonance, the gap appears in almost the same position as Figure 2.2, but with slight enlargement. In addition, thanks to the double lead cores, the maximum predicted attenuation in this case is 54.8dB as compared to 33.3dB of attenuation for the previous case. However, as shown in Figure 2.8, unlike a traditional Bragg scattering band gap, several peaks appear within the gap width.

2.2.1 Local resonance derived lower frequency band gap

To demonstrate that the lower frequency band gap is due to local resonance, modal analysis of the given structure was performed. The existence of local resonance could be verified by the presence of a discrete or a continuous mode associated with the coated double lead cylinders. For our CDHL structure, it is expected that the low frequency band gap at 7 kHz in Figure 2.8 corresponds to local resonance. This could be supported by looking at the mode shapes of a single cell both at the upper edge and the lower edge of the band gap.

In Figure 2.9 and Figure 2.10, the FEA demonstrates localized discrete resonant behavior within the circular scatterers at the lower and upper edge frequencies of the band gap. Figure 2.9 corresponds to the displacement field at the lower frequency edge of the band gap. It is easy to Figure out that the energy is harvested in the double cylinders, whereas in Figure 2.10, the energy is localized in the rubber coating. Therefore, by introducing the double lead cylinders, the energy could be localized in the cylinders, which leads to a generation of a band gap. Hence, it is proved that the lower frequency band gap is generated due to local resonance.

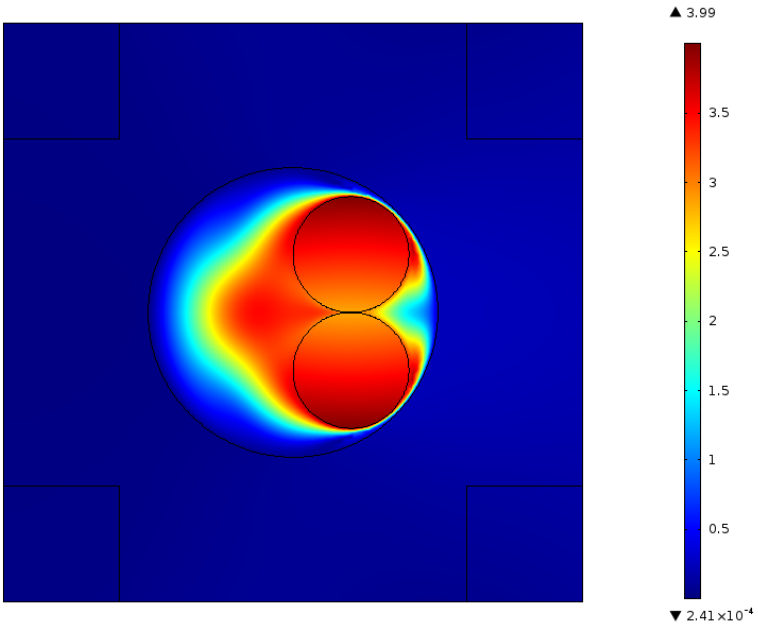

Figure 2.9 Mode shape at *f*=6790.7 Hz of the band gap

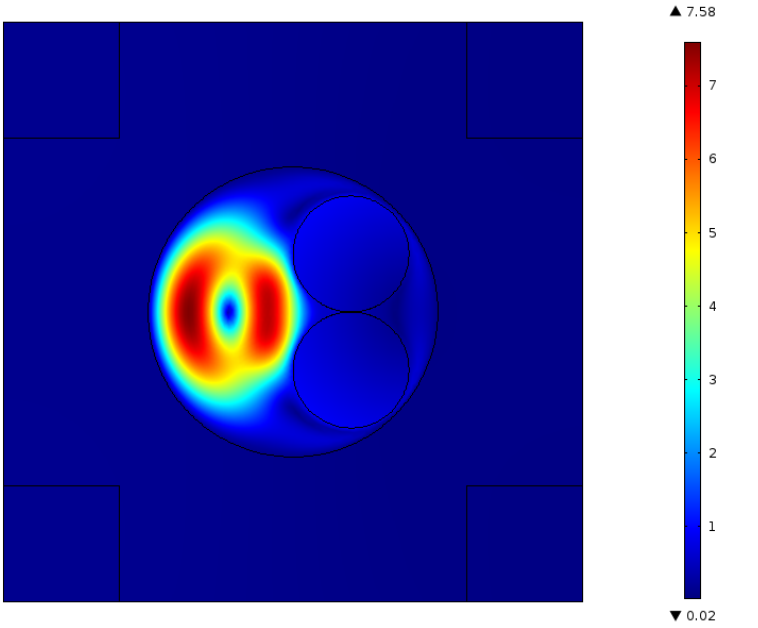

Figure 2.10 Mode shape at *f*=7165.9 Hz of the band gap

2.2.2 Interference between Bragg scattering band gap and local resonance band gap

According to the unusual results obtained in Figure 2.8, where a large band gap appeared at high frequency with a couple of peaks in the gap width, it is necessary to understand where the peaks in the gap width come from and whether it is due to the interference between the Bragg scattering band gap and the local resonance band gap. Hence, to better distinguish the local resonant band gap from Bragg scattering band gap, we carried out modal analysis and examined the phase spectrum of the structure.

In the higher frequency range of 70-95 kHz, several peaks appear. Repeating the previous procedure, a numerical modal analysis was performed and several localized resonances within the rubber substrate were observed in the higher transmission gap width that corresponded to peaks appearing in the transmission spectrum.

Quite different from lumped resonances found in the local resonance gap range, these are continuous modes. Some examples of these continuous modes are shown in Figure 2.11 and Figure 2.12. The energy is localized in the rubber coating, and it is the lower modulus (as compared to epoxy) of the rubber that has introduced these continuous modes. Hence, it is proved that multiple local resonances occur within the gap width.

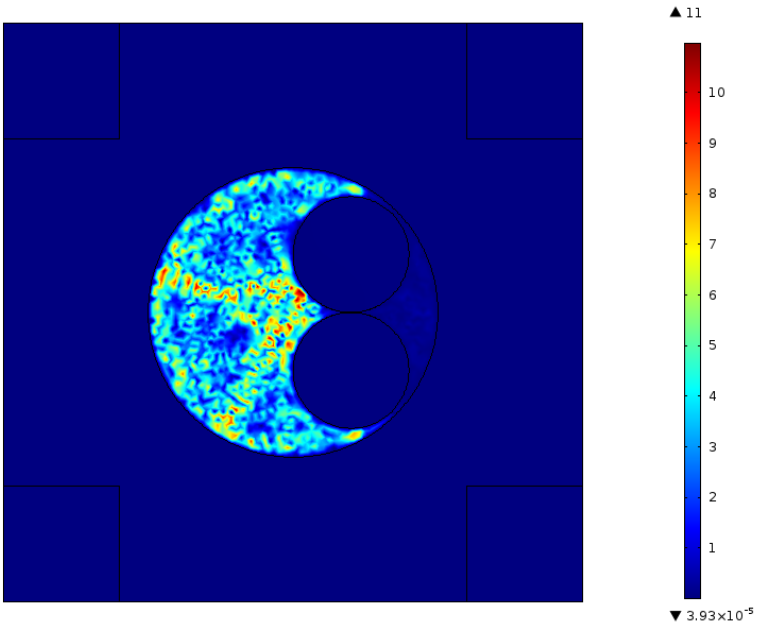

Figure 2.11 Example of higher continuous modes at *f*=80882 Hz

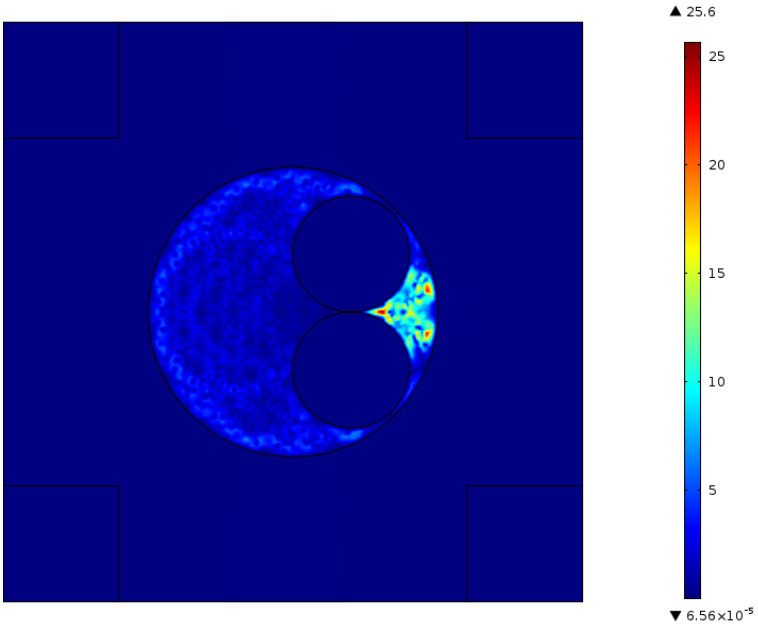

Figure 2.12 Example of higher continuous modes at *f*=81795 Hz

To prove the existence of wave scattering in the gap width, we examined the phase spectrum of the structure. In this case, for better transfer of energy into the phononic crystals,

waves were excited and measured in water on either side of the structure. The phase spectrum was tested in water because, quite different from the epoxy background where both transverse waves and longitudinal waves exist, only longitudinal phase spectrum is tested in water. The phase was computed between the input location and either points C or D in the water at the front or back of the structure, respectively (see Figure 2.13). As discussed in reference [40], if there is no scattering in a frequency band, a linear phase response would be observed at both measurement points, corresponding to the propagation delay between the input position and respective measurement point. However, where there is wave scattering, the phase taken before the structure (pt. C) would remain constant, whereas the phase spectrum taken after the structure (pt. D) is no longer linearly decreasing. Examples of phase spectra are given in Figure 2.14 and Figure 2.15, which will be discussed below.

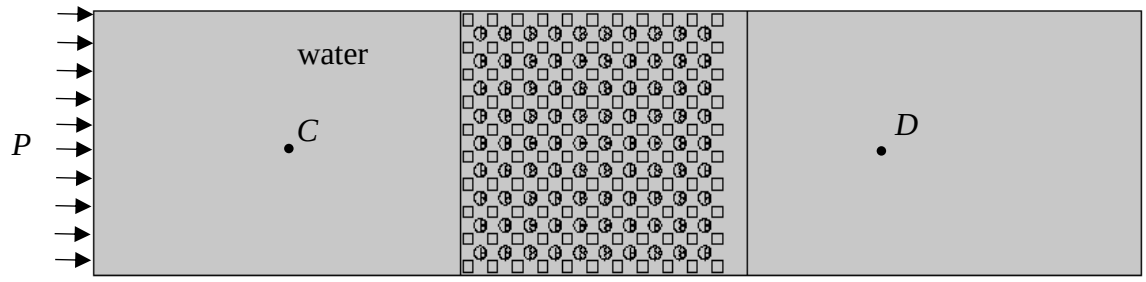

Figure 2.13 CDHL structure with measurement points C and D in water

Shown in Figures 2.14 and Figure 2.15 are the phase spectra taken at points C and D, respectively. It is quite clear that in the gap region, the phase taken at point C remains constant and the phase taken at point D is no longer linearly decreasing. These facts have demonstrated that within the bandwidth, apart from multiple local resonances, there is also Bragg wave

scattering. As a result, the gap generated in the higher frequency region is actually a result of the interference of both Local Resonance and Bragg Scattering.

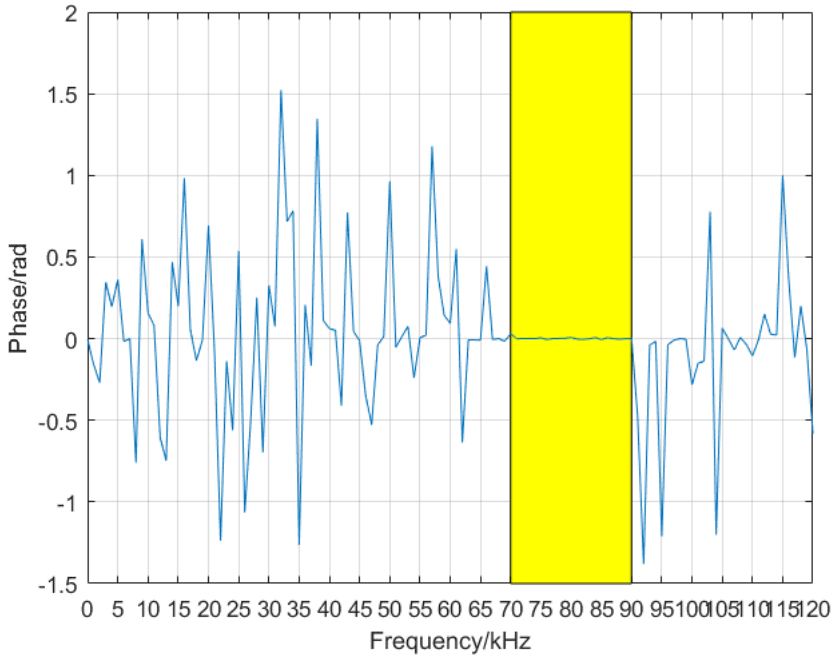

Figure 2.14 Phase taken at point C of CDHL

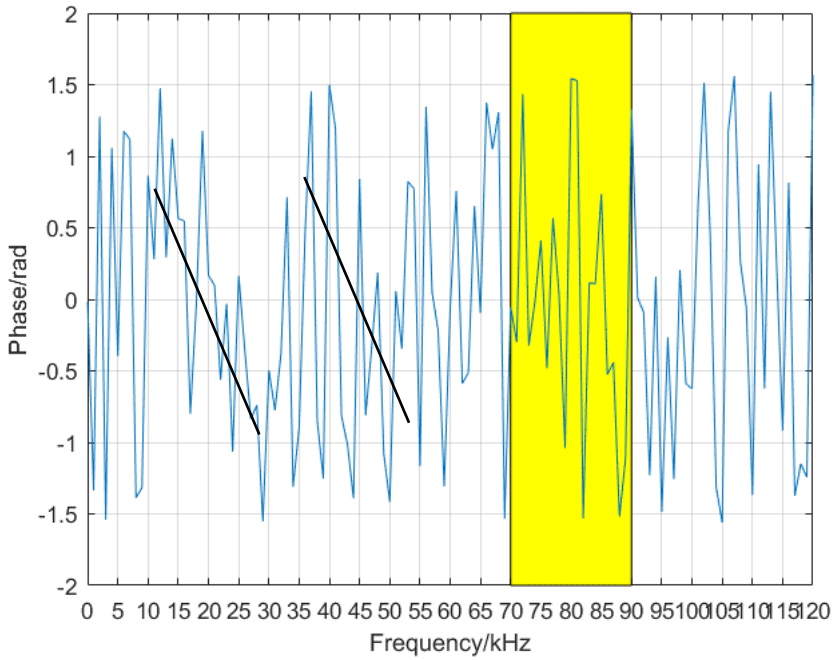

Figure 2.15 Phase taken at point D for the CDHL

2.2.3 Case study

To better understand and clarify the problem, more cases need to be studied for comparison purposes. These cases should include single lead cylinder, uncoated double lead cylinder and single rubber cylinder.

2.2.3.1 Single lead cylinder

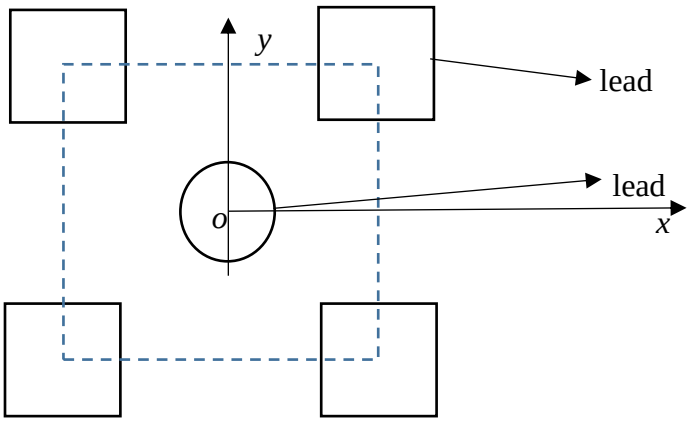

Figure 2.16 Schematic of unit cell of single lead coating structure

To begin with, the single lead cylinder is illustrated in Figure 1.18. It is a case that has been studied in the literature. The transmission spectrum corresponding to the structure is shown in Figure 2.17.

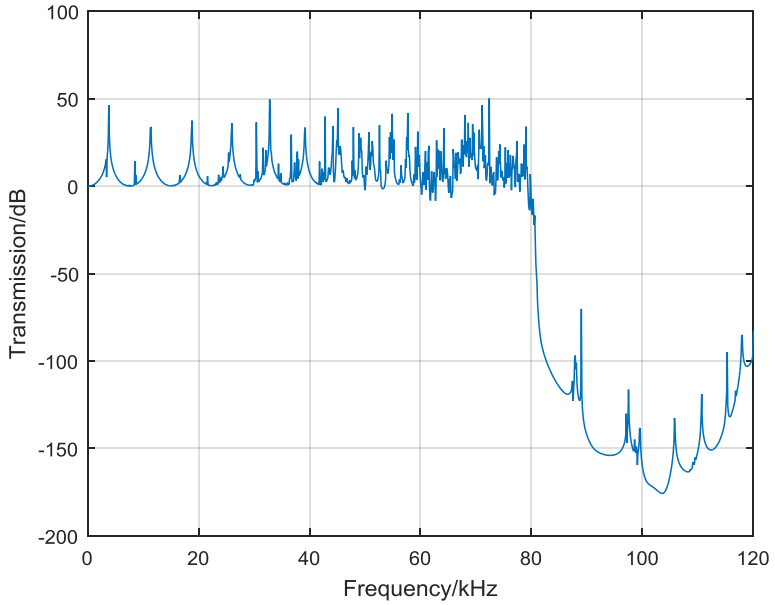

Figure 2.17 Transmission with single lead coating without core

It is quite clear from the results that there is only one band gap, which is situated at upper frequencies. We do not see any band gaps in the lower frequency range. Then, the phase study is carried out following the previous procedure. In the higher frequency range, the relative phase taken at point C is observed to be constant as shown in Figure 2.18. At the same time, the relative phase taken at point D is no longer linearly decreasing as demonstrated by Figure 2.19.

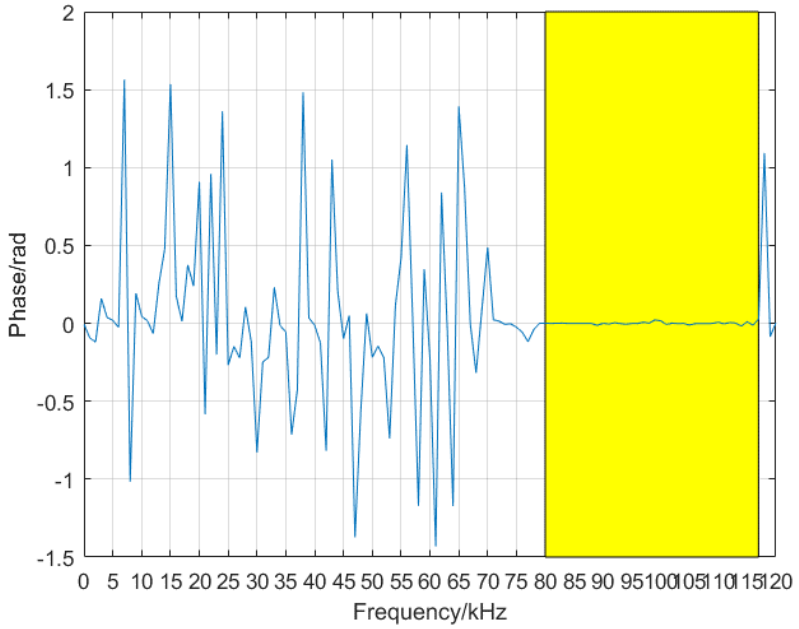

Figure 2.18 Relative phase spectrum taken at point C

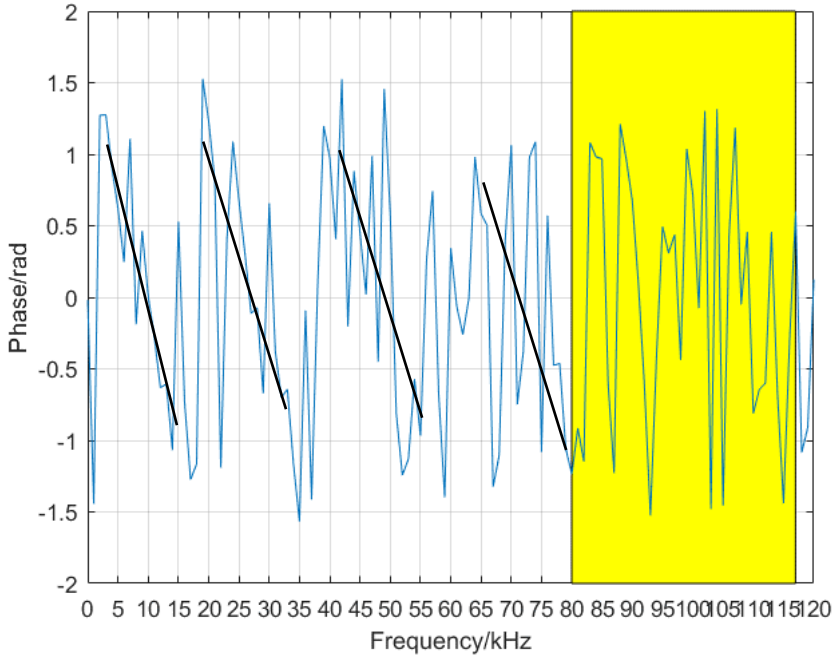

Figure 2.19 Relative phase spectrum taken at point D

To examine whether there are local resonances in the higher band width, a modal analysis is also carried out. According to our calculation, no modes are found in the gap width, so there is no local resonance happening within the gap width.

2.2.3.2 Single rubber cylinder

The single lead cylinder case discussed before has proved the effectiveness of the method where the phase calculation serves as an indicator of the existence of Bragg scattering and the modal analysis as an indicator for the existence of local resonance. Next, we examine the case where the single cylindrical lead scatterer is replaced by a solid rubber one, as Indicated in Figure 2.20.

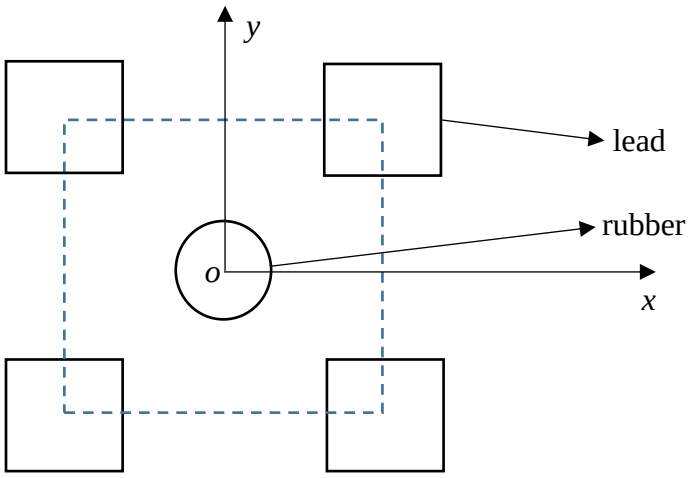

Figure 2.20 Schematic of the structure with only one rubber cylinder in the center

Shown in Figure 2.21 is the corresponding transmission with the rubber cylinder in the center.

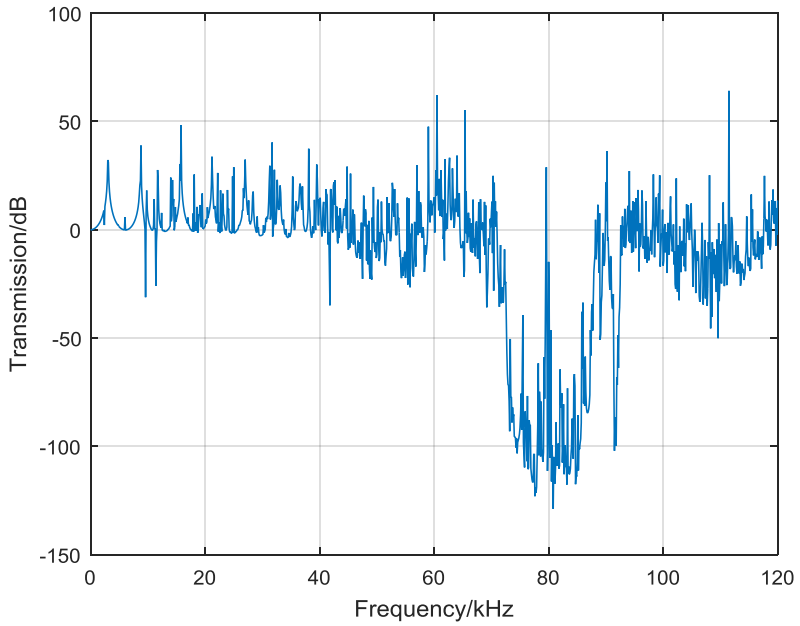

Figure 2.21 Transmission with only one rubber cylinder in the center

In this case, the wave is scattered among square rods and cylinders and has successfully generated a band gap between 70-90 kHz. But within the gap width, several peaks also appear. According to our modal analysis results, several vibration modes are found in this higher frequency gap region indicating the appearance of several local resonances. In the previous cases when we look at the phase spectrum in the gap region, shown in Figure 2.22 and Figure 2.23, the phase remains constant at point C, yet is no longer linearly decreasing at point D.

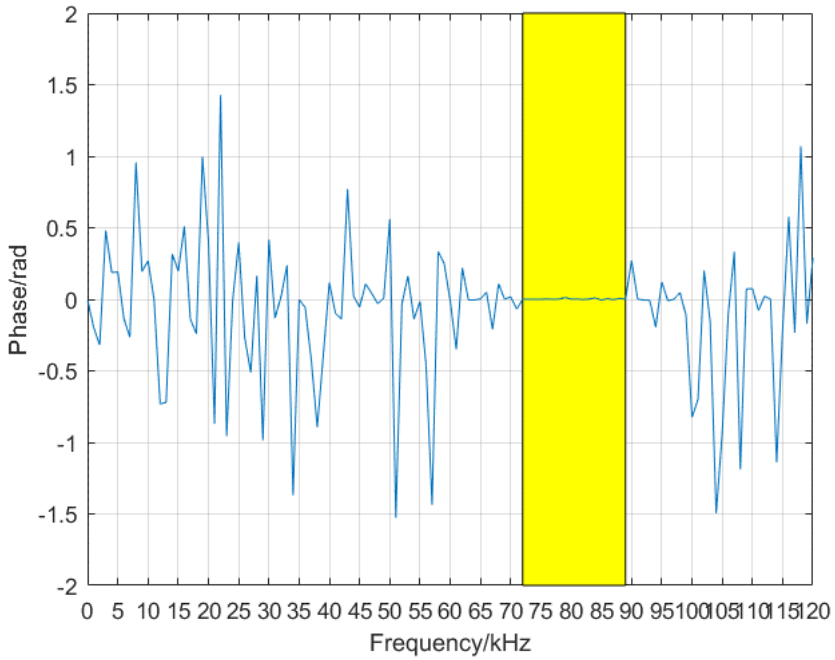

Figure 2.22 Relative phase taken at point C for the pure rubber coating structure

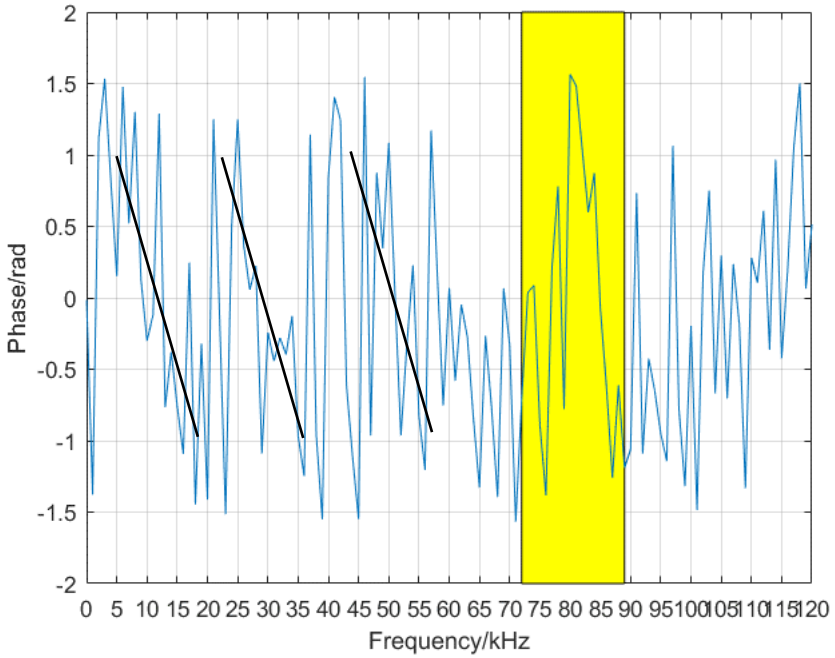

Figure 2.23 Relative phase taken at point D for the pure rubber coating structure

2.2.3.3 Uncoated double lead cylinder

After that, a double-cylinder structure without any rubber coating is also considered. The schematic of the structure with no coating is shown in Figure 2.24 whereas the transmission spectrum is indicated in Figure 2.25

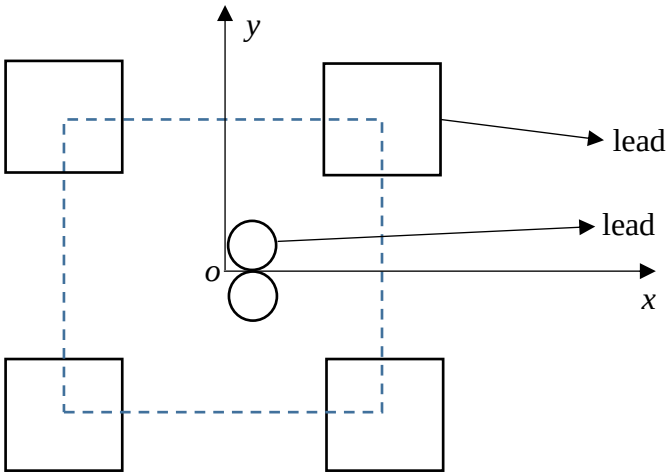

Figure 2.24 Schematic of structure with no coating

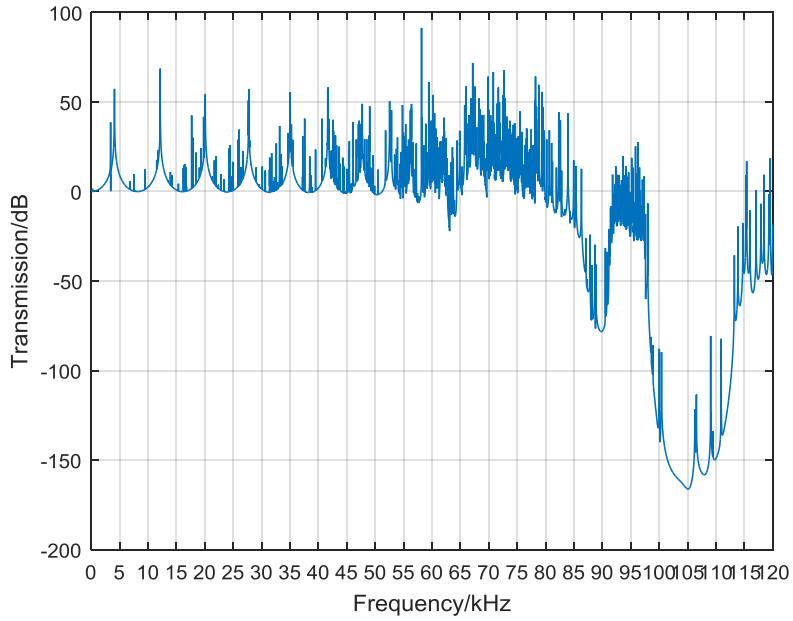

Figure 2.25 Transmission spectrum with no rubber coating around double cylinders

This time, according to Figure 2.25 shown above, two band gaps appeared in the high frequency range. According to our modal analysis, no modes are found in either band gap. At the same time, the phase spectrum obtained in Figure 2.26 and Figure 2.27 clearly demonstrate that in the gap width, the phase is relatively constant at the front (pt. C) within the gap band and no longer linearly decreasing, but rather oscillating within $+\pi$ and $-\pi$ when measured at the back (pt. D).

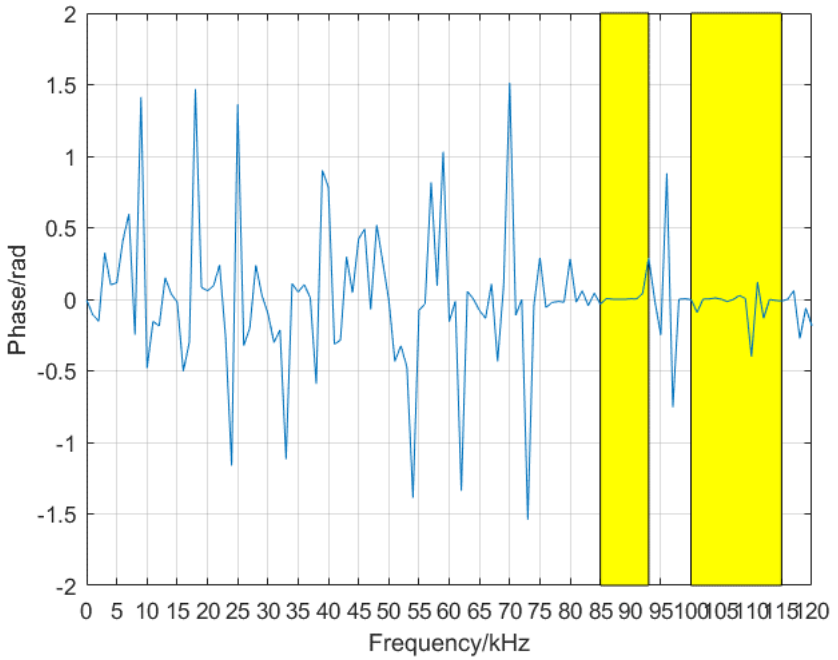

Figure 2.26 Relative phase taken at point C for a double lead core structure without coating

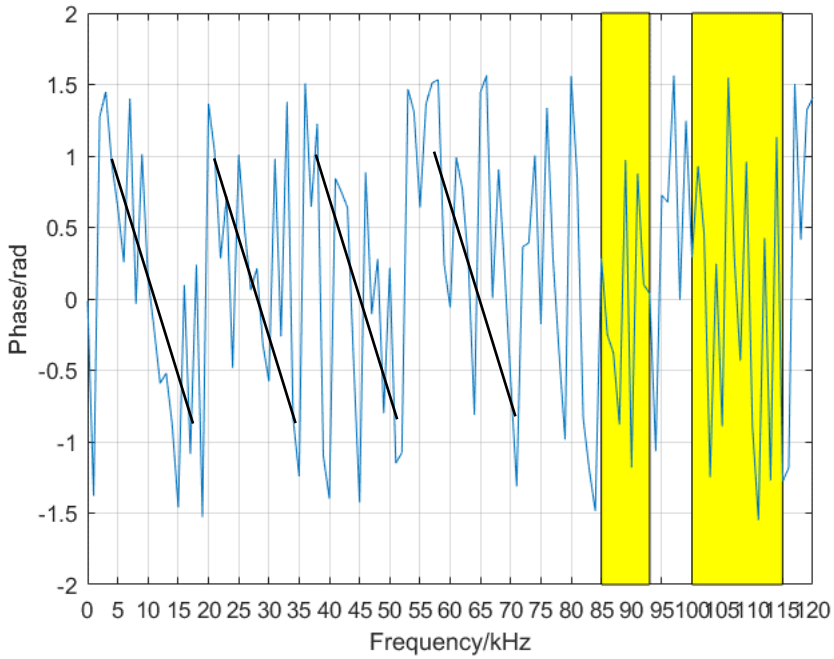

Figure 2.27 Relative phase taken at point D for a double lead core structure without coating

2.2.4 Position effects of double lead cores with rubber coating on the band gap structure

Finally, it is further investigated how the *x* position of the small circular scatterers with rubber coating will affect the band gap, specifically the local resonant band gap. Cartesian coordinates are assigned with the origin at the center of the large rubber circular scatterers. It can be seen from Figure 2.5 that the double circular scatterers are symmetrical about the *x* axis. Hence, the *x* position of the coated double scatterers is varied from (-0.001, 0) to (0.001, 0), as shown in Figure 2.28.

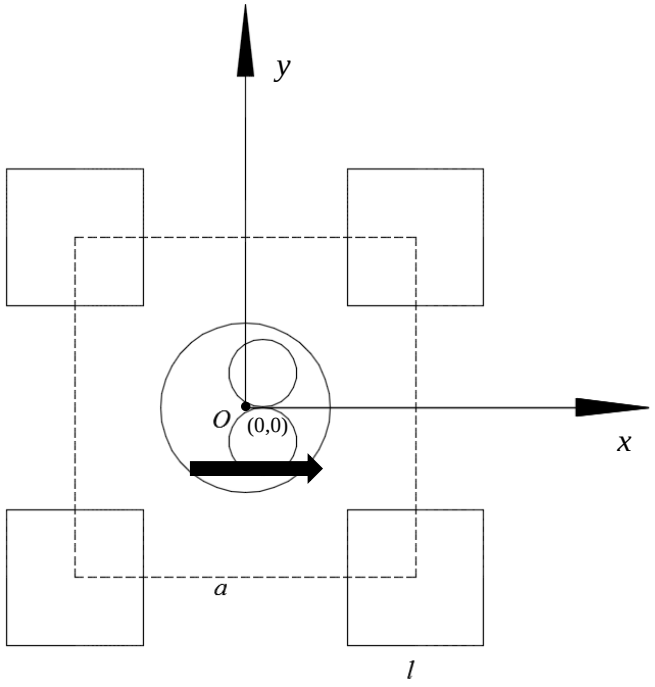

Figure 2.28 Schematic of the variation of the central lead core

The corresponding variation of transmission is presented below in Figure 2.29.

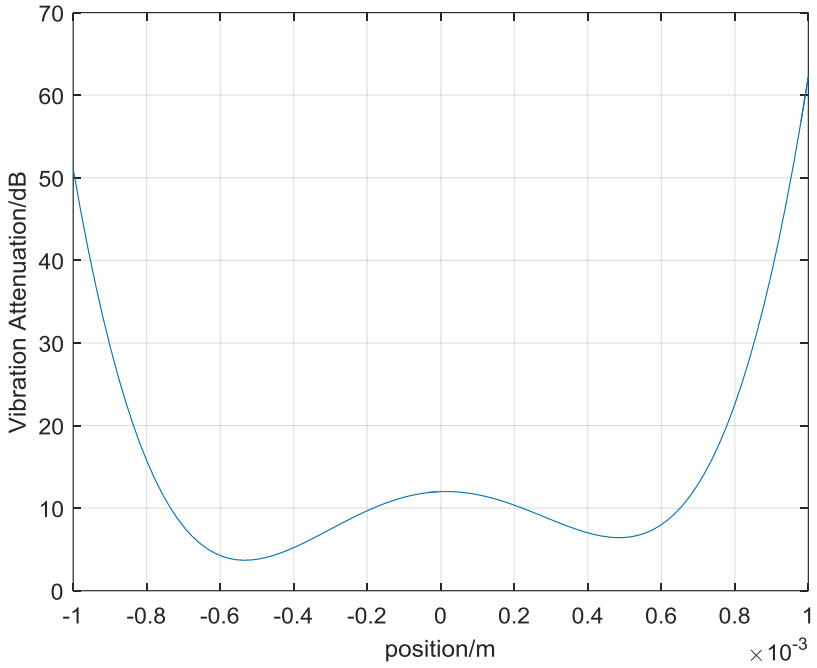

Figure 2.29 Variation of transmission with respect to the varied position of double circular scatterers

We can see from Figure 2.30 that a nearly symmetrical plot is presented. The maximum attenuation appears at the two edges, that is, at (-0.001,0) and (0.001,0), where the two lead cylinders are nearly tangent to the inner circular surface of the epoxy matrix.

3.0 PROPOSED STRUCTURE FOR ENGINEERING APPLICATION

The discussion in the previous chapters enables us to visualize how and where the band gap structure would be generated by fabricating the proposed structure. Theoretically speaking, due to the existence of the rubber coating, there are resonances between the double lead cores and the rubber coating, which make the existence of band gap possible. At the same time, all the scatterers are arranged periodically so that when the wavelength is of the same order as the lattice constant, Bragg scattering effect takes place. Therefore, under a specific condition, a traditional Bragg scattering derived gap develops. In the meantime, by carrying out modal analysis and phase calculations, we identified the formation mechanism that lies behind the phenomenon, which provided us a hint of how we may control the position of the band gap. Therefore, in this chapter, from a practical engineering prospective, we will discuss possible ways to control the band gap position so as to possibly attenuate the vibration of the entire investigated frequency range (0-120 kHz).

According to different frequencies of vibration that are attenuated by the structure, the engineering design would be divided into three categories: high frequency design, medium frequency design and low frequency design.

3.1 HIGH FREQUENCY ATTENUATION DESIGN

By high frequency, we mean the ultrasonic vibration with frequencies in the range of 40-120 kHz. From a physics point of view, due to the existence of rubber coating, the generation of the gap would be due to the interference of the local-resonance theorem and Bragg-scattering theorem as stated in the previous introduction chapters. However, in this chapter, we would like to control the band gap position so as to enable the structure to attenuate the vibration of the entire high frequency range. In the Introduction chapter, it is clearly stated that the Local resonance derived gap will be affected by the material parameters of the core and the coating. To modify the band gap structure, one has to change the material parameters, which in practice, is equivalent to changing the type of material; this may cause inconvenience. However, if the Bragg scattering band gap is to be modified, apart from material parameters, geometries of the lattice would also have clear impact on the position as well as the width of the band gap. The geometries indicated here include lattice constant, side length of the square scatterers, rotation of the non-circle scatterers, etc. Since changing the geometries of the lattice is easier to achieve in reality, the modification of the Bragg scattering band gap is the main target for achieving our object in this section.

Therefore, to attenuate the high frequency vibration, we examine the original proposed structure in Figure 2.4. According to our simulation, with the increase of the side length of square scatterers, the Midgap will decrease. In other words, by enlarging the square scatterers, the band gap will move towards a lower frequency range. Recall that the goal in this section is to attenuate ultrasonic vibration with frequencies from 40-120 kHz, we will arbitrarily set the side length of the square scatterers as l=0.004 m. Meanwhile, to better illustrate the problem, we introduced a non-dimensionalized lattice constant

$$N = \frac{Lattice\ Constant}{Side\ length\ of\ the\ square\ scatterers} \tag{3-1}$$

which is intended to describe how the lattice constant will affect the band gap structure. Simultaneously increasing the lattice constant and rotating the square scatterers, the resultant band structure is shown in Figure 3.1 and Figure 3.2.

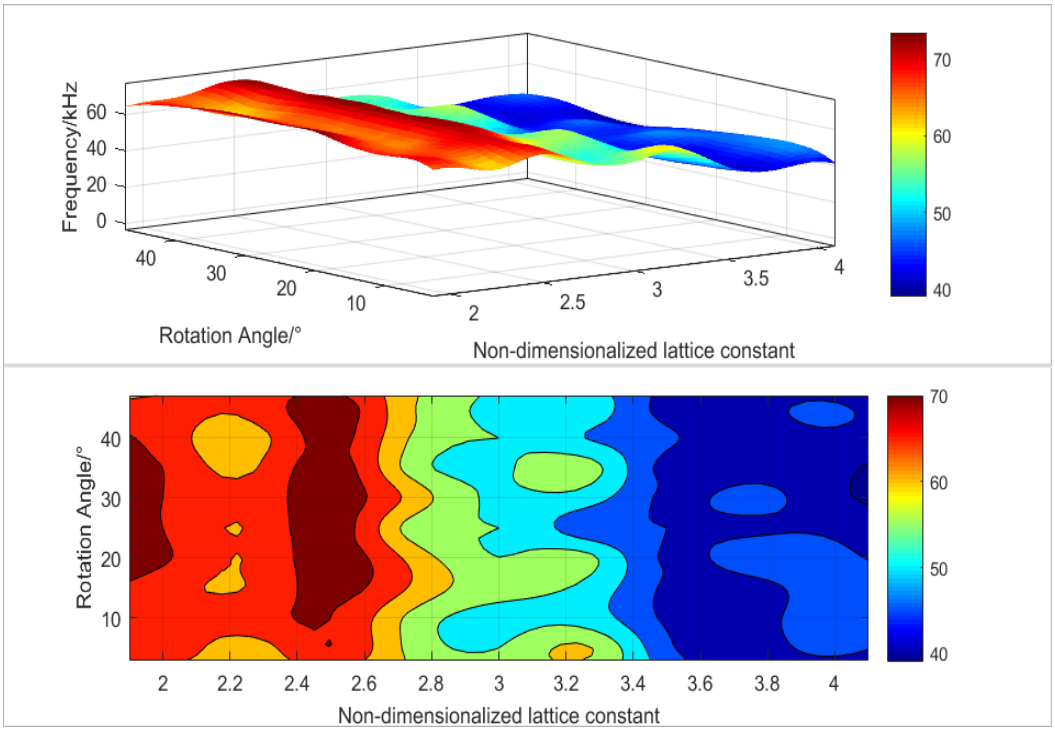

Figure 3.1 Lower band variation with respect to rotation angle and lattice constant variation when *l*=0.004m

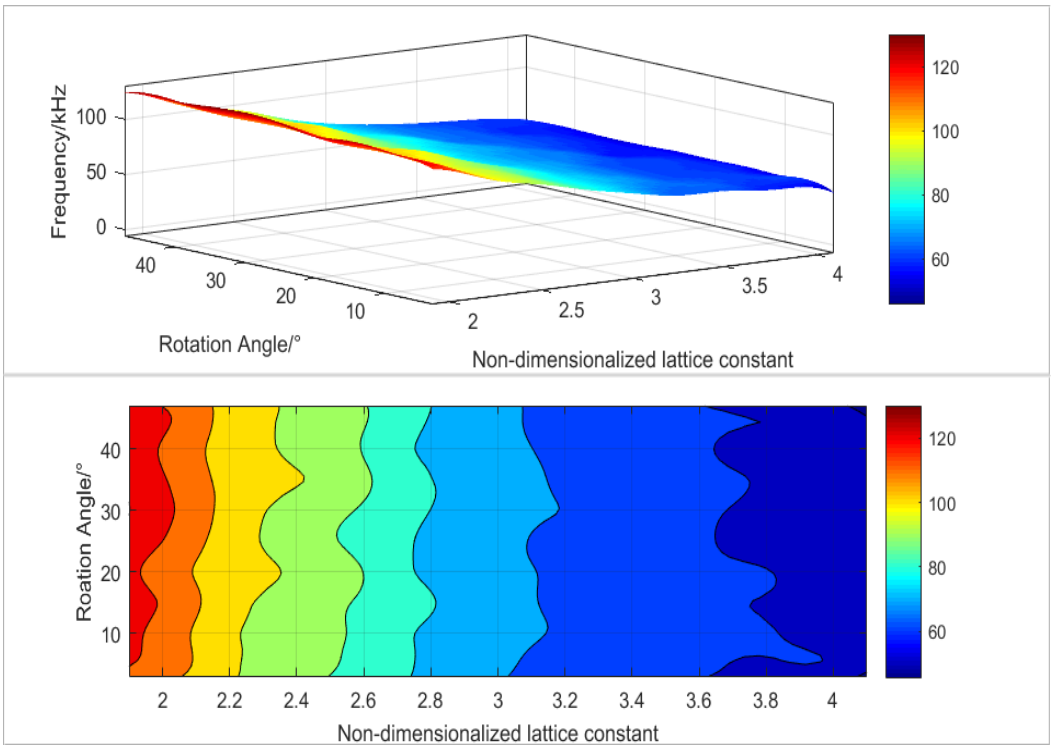

Figure 3.2 Higher band variation with respect to rotation angle and lattice constant variation when *l*=0.004m

In Figure 3.1 and Figure 3.2, the upper curve represents the upper bound whereas the lower curve stands for the lower bound of the band gap. From the results, it is easy to see that with the increase of the non-dimensionalized lattice constant from 2 to 4, both the upper band and the lower band tend to shift towards the lower frequency range. In other words, if higher frequency vibration is to be attenuated, one would need to fabricate a structure with a smaller lattice constant whereas if a lower frequency vibration is to be attenuated, a larger lattice constant should be considered. On the other hand, when the non-dimensionalized lattice constant is set at some specific frequencies, moderate change will take place with the increase of rotation angle; that is, the lattice constant will have a more obvious effect on the band position compared with the rotation angle variation. This is proved more clearly by the midgap in Figure 3.3

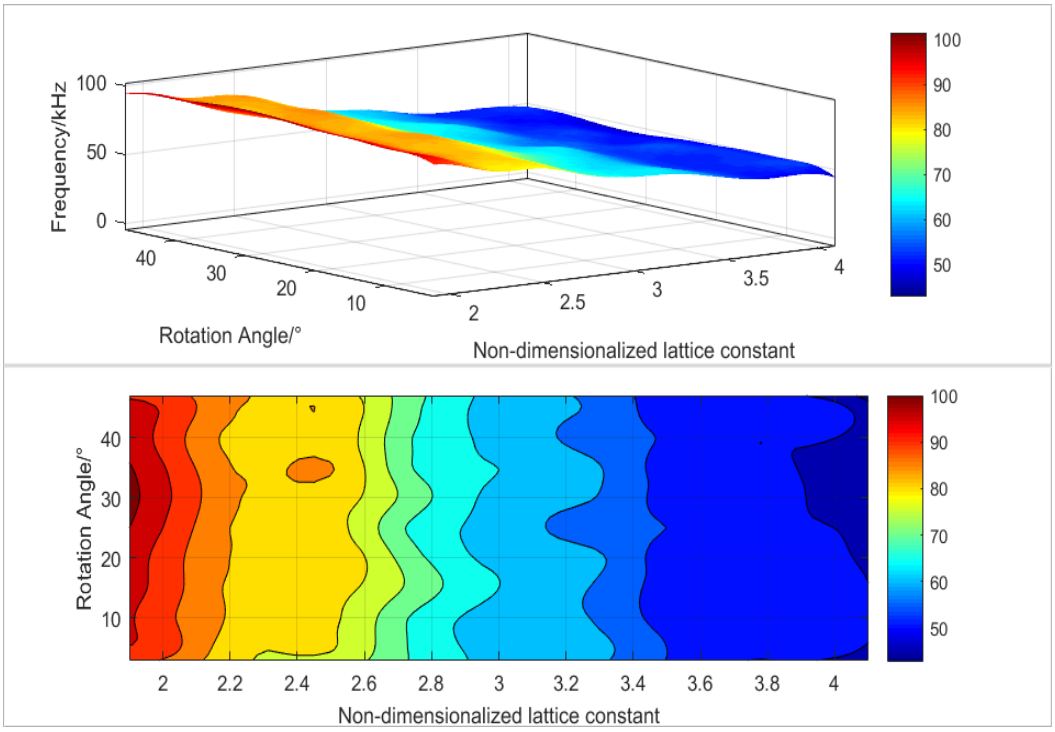

Figure 3.3 Midgap variation with respect to rotation angle and lattice constant when *l*=0.004 m

Figure 3.3 is more straightforward in that not too much change will take place in the position of the band gap by rotating the square scatterers as compared with that caused by the non-dimensionalized lattice constant variation. Moreover, with the increase of the lattice constant, the slope of the midgap decreases, which means that the midgap is more sensitive to a small lattice constant than to a large lattice constant. Also, to have a more straightforward vision of the gap width with respect to the changing lattice constant and the rotation angle of the square scatterers, we have come up with Figure 3.4.

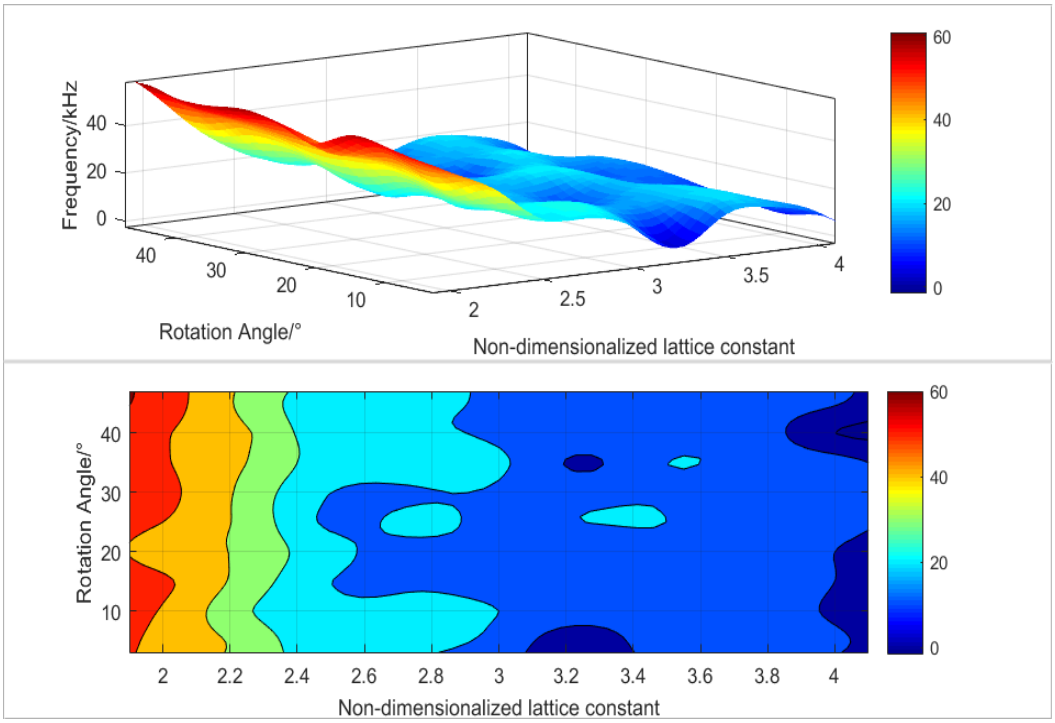

Figure 3.4 Gap width variation with respect to changing rotation angle and lattice constant when *l*=0.004 m

From Figure 3.4, quite similar to the midgap variation, the lattice constant will have a clearer impact than the rotation angle on the gap width. Meanwhile, corresponding to the increasing non-dimensionalized lattice constant, the gap width decreases, in other words, a narrower band gap will be obtained when fabricating the structure with a greater lattice constant. Also, similar to the previous midgap case, the slope of the band gap decreases; that is, the gap width is also more sensitive to lattice constant structure than it is to large lattice constant structure.

Therefore, previous results have indicated how one could attenuate specific high frequencies of the vibration mainly by increasing the lattice constant. By fabricating structures with a large lattice constant, a narrower gap width would be obtained but the entire gap would

appear in a rather lower frequency area. By coming up with lower lattice constant structures, the gap may appear in a higher frequency area but a wider gap width would be obtained.

3.2 MID-FREQUENCY ATTENUATION DESIGN

We refer to the vibration with mid-frequency as vibration with 10-60 kHz frequencies that belong to the ultrasonic and audible vibration ranges. Following the procedure illustrated in section 3.1, we also decided to modify the Bragg scattering band gap by changing the geometries of the lattice. This time, the side length of the square scatterers is arbitrarily set as l=0.01 m. Following the same procedure in Section 3.1, by varying the lattice constant as well as the rotation angle of the square scatterers, we have first come up with the band structure as shown in Figure 3.5 and Figure 3.6.

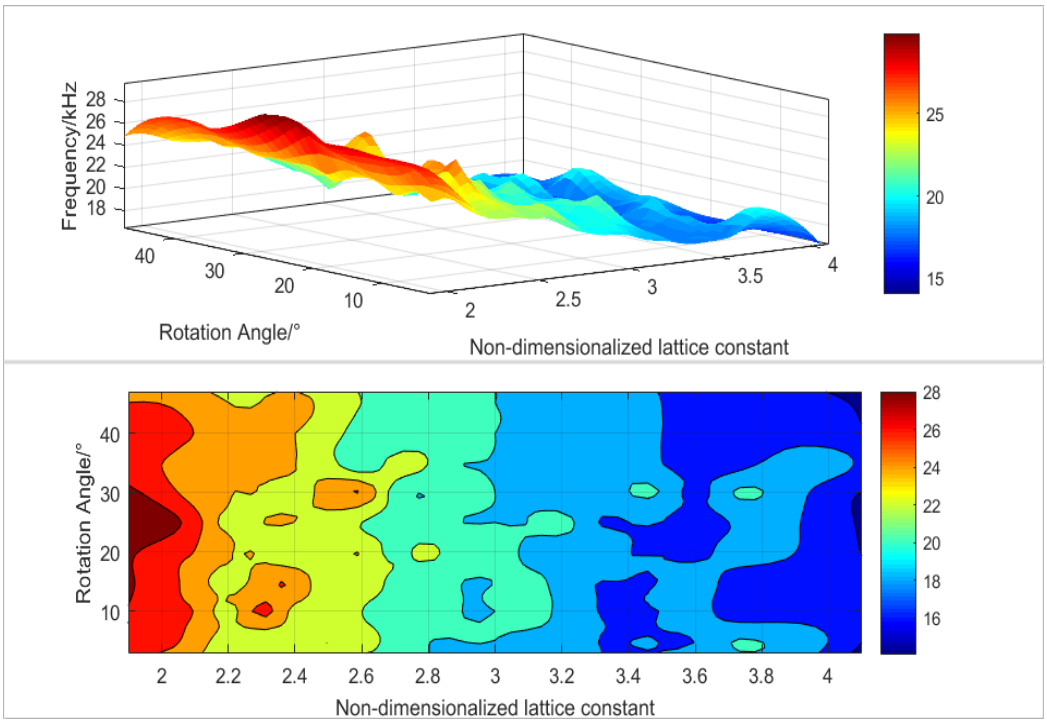

Figure 3.5 Lower band variation with respect to rotation angle and lattice constant variation when *l*=0.01 m

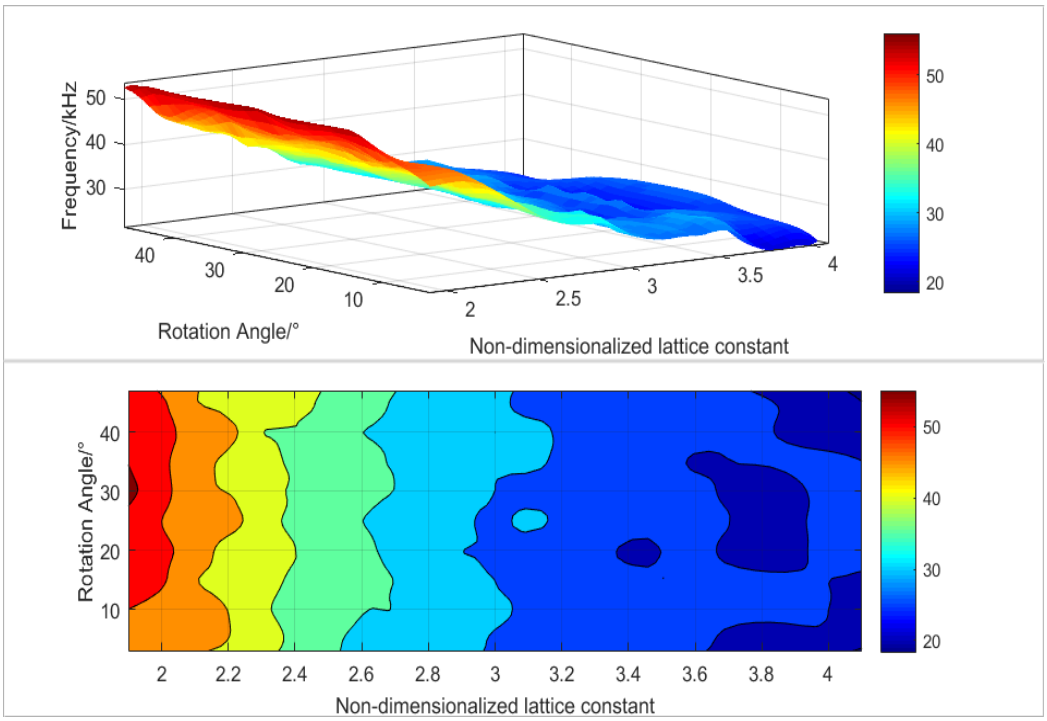

Figure 3.6 Higher band variation with respect to rotation angle and lattice constant variation when *l*=0.01m

As illustrated in Figure 3.5 and Figure 3.6, the upper curve corresponds to the upper limit of the band gap whereas the lower curve corresponds to the lower limit of the band gap. It is quite similar in trend to the high frequency design in Sec. 3.1, in that when compared to the rotation angle, the lattice constant has a clearer impact on the position of the band structure. To better visualize how the position of the band gap changes with the rotation angle and the lattice constant, we have come up with a midgap variation plot, as shown in Figure 3.7

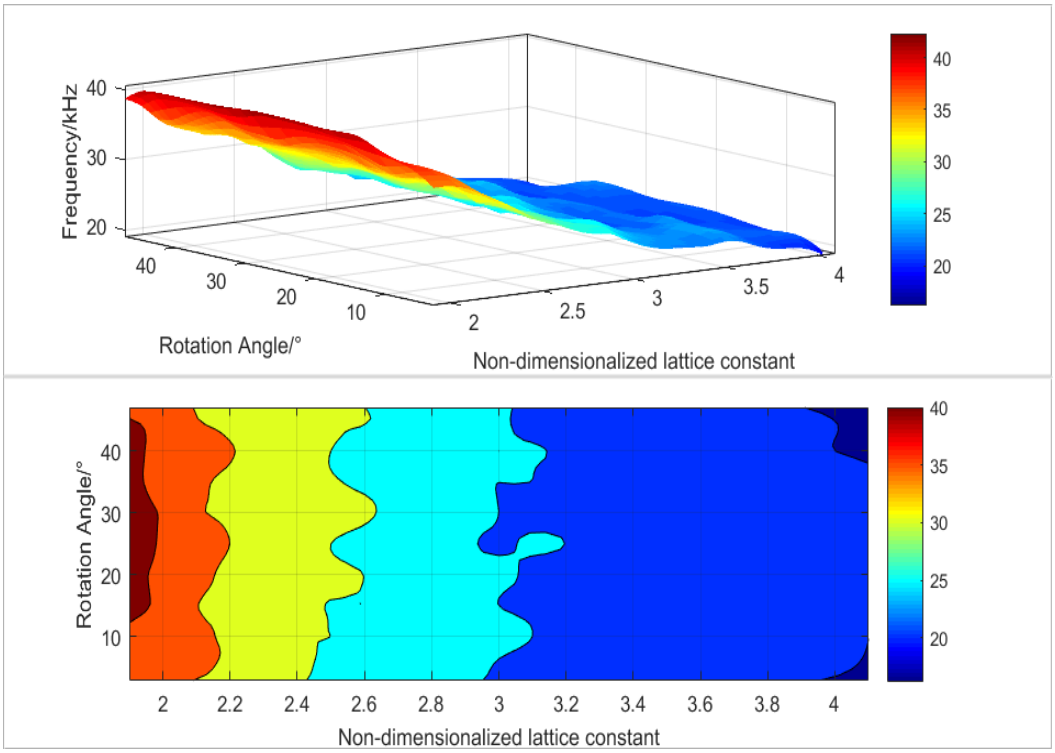

Figure 3.7 Midgap variation with respect to the changing rotation angle and lattice constant when *l*=0.01 m

From Figure 3.7, it is easy to discover that when the side length of the square scatterers is set as *l*=0.01 m, the whole band gap structure is shifted towards a lower frequency region. By increasing the non-dimensionalized lattice constant from 2 to 4, the Midgap decreases from 40 kHz down to 20 kHz. In the meantime, the variation of the Midgap decreases with the increase of the non-dimensional lattice constant. Specifically, when the non-dimensionalized lattice constant varied from two to three, the Midgap more severely decreases, as compared to the case when the non-dimensionalized lattice constant varied from three to four. Also, in this case, the variation of rotation angle will not have clear impact on the position of the band gap structure. Moreover, as seen in the gap width variation plotted in Figure 3.8, by raising the non-dimensionalized lattice constant, the gap width is monotonically decreasing, with a few bumps.

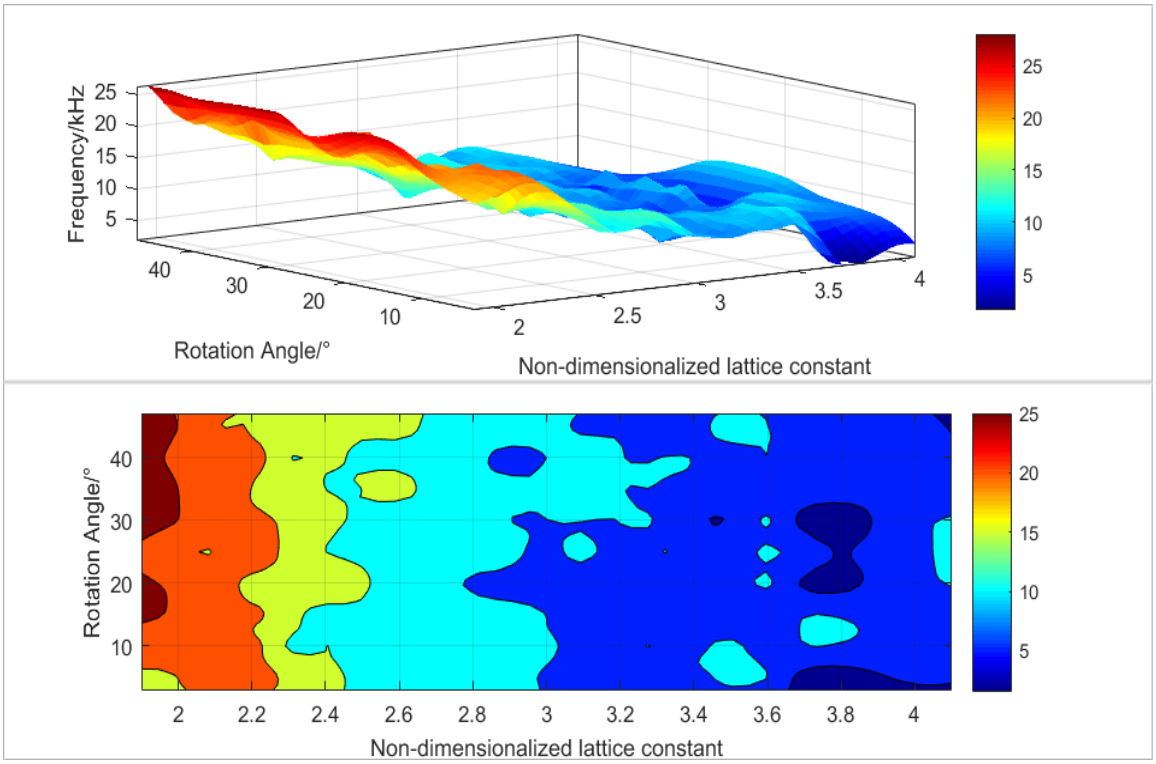

Figure 3.8 Gap width variation with respect to changing rotation angle and lattice constant when *l*=0.01 m

At the same time, the lattice constant has a clear impact on the gap width. With the increase of the non-dimensionalized lattice constant, the band width decreases. However, it is interesting to note that several peaks appear in the contour plot of Figure 3.8. In other words, when the non-dimensionalized lattice constant is fixed between 3.4 and 3.8, at some specific rotation angle, the band gap can be enlarged or narrowed.

To sum up, the results provided in section 3.2 have given us a hint of how we can possibly design specific structures so as to attenuate vibrations that lie in the mid-frequency region. First of all, by using larger square scatterers, the whole band gap is shifted towards a lower frequency region. Meanwhile, similar to the previous high frequency case, compared with rotating the scatterers, increasing/decreasing the lattice constant is more effective for modifying

the band gap structure. More specifically, with a larger lattice constant, although lower frequency band gaps will be obtained, those gaps are narrower. Conversely, if a rather high frequency band gap is to be obtained, one will expect to a wider gap.

3.3 LOW FREQUENCY ATTENUATION DESIGN

In previous sections, several discussions were carried out and a couple of proposals were provided to fabricate specific structures so as to attenuate ultrasonic vibrations with specific frequencies. Since in all the previous cases, the wavelength of the vibration is of the same order as the lattice constant, one has to make use of the Bragg scattering theorem to attenuate the vibration. However, when the vibration reaches the audible frequency range, especially lower than 10 kHz frequency, one has to use the local resonance derived gap. This is simply because, in this case, the wavelength is much greater than the lattice constant. If a Bragg scattering derived gap is used to attenuate the vibration, one will have to fabricate a large structure to make the lattice constant of the same order as the wavelength which, from a practical engineering perspective, will result in too much waste.

Unlike Bragg scattering band gap formation mechanism, the formation of the local resonance band gap is due to the resonance between the double lead core and the rubber coating. It has nothing to do with the geometries of the lattice. Therefore, the most convenient way to change the behavior is to modify the material parameters of the rubber coating. By looking through the material parameters of the rubber, it is found that many kinds of rubber exist. They are with a similar density but different Young's moduli. From a practical engineering prospective, we would expect the modification of Young's modulus to be the most convenient

mechanism for tuning the band gaps. Therefore, we have investigated how the Young's modulus would affect the band gap both in position and in width as shown in Figure 3.7.

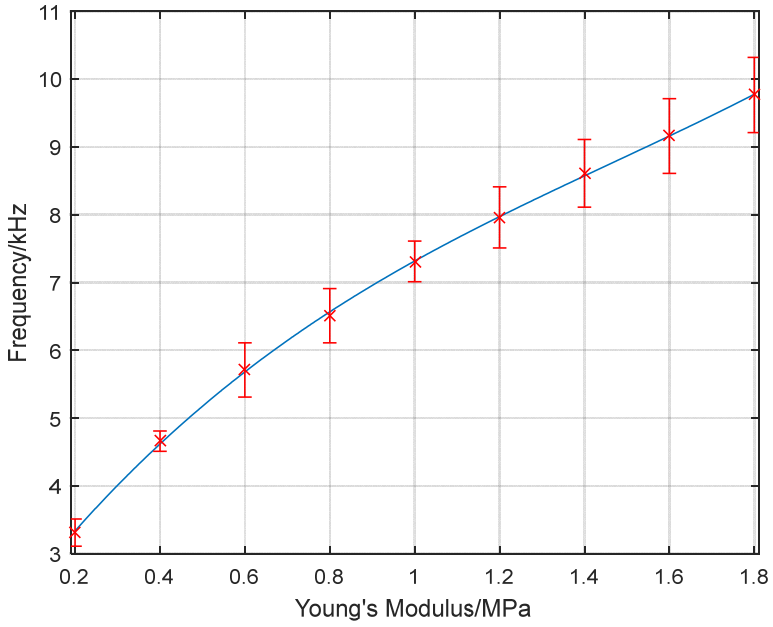

Figure 3.9 Midgap variation with respect to the changing Young's Modulus

Figure 3.7 is a plot with an error bar. The upper limit indicates the upper edge of the gap and the lower limit indicates the lower edge of the gap. The difference between the upper limit and the lower limit would refer to the band gap we want. As indicated in Figure 3.7, by increasing the Young's modulus of the rubber coating, the band gap monotonically shifts towards high frequency; that is to say, if one would like to obtain a lower frequency band gap, a softer rubber would be considered. Also, if a higher frequency band gap is required, a stiffer rubber should be used. Therefore, for the ordinary engineering rubbers whose Young's modulus lie in the range of 0.2-1.8 Mpa, one can tune the band gap within the range of 3-9.5 kHz.

Meanwhile, Figure 3.7 has presented a plot which is similar to a square root plot. This can be supported by the fact that the lower frequency band gap is tuned by the local resonance between the lead core and the rubber coating. The natural frequency for a lumped spring-mass can be expressed as

$$\omega_n = \sqrt{\frac{k}{m}} \tag{3-1}$$

where the stiffness in this case is a function of the Young's modulus. Therefore, corresponding to the variation of the Young's Modulus, the Midgap should be change as observed.

To have a direct visualization of the gap width variation, we have come up with Figure 3.8.

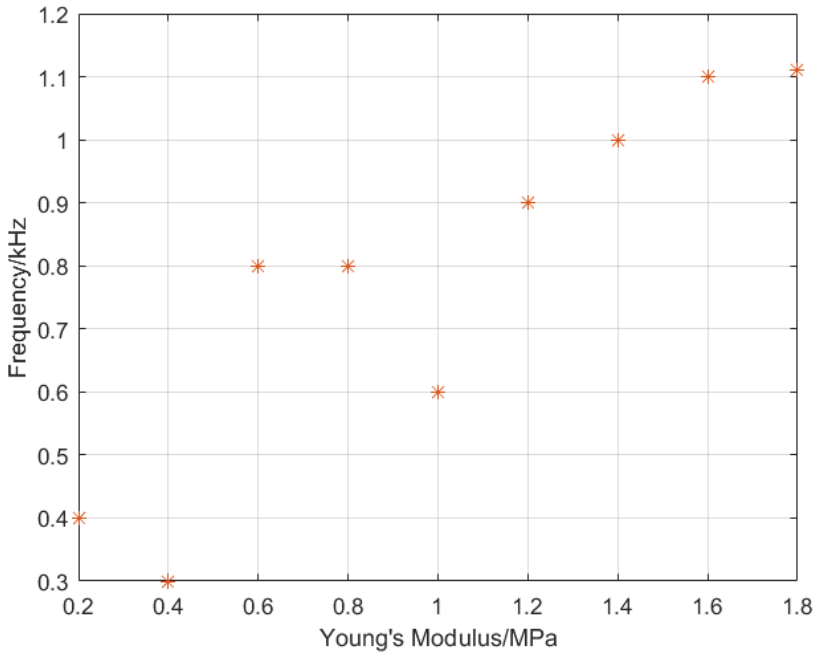

Figure 3.10 Gap width variation with respect to the changing Young's Modulus

As the rubber coating gets stiffer, generally speaking, a wider gap will be obtained. However, unlike the previous cases, the gap width is not monotonically increasing with an increase in Young's modulus.

4.0 EXPERIMENTAL STUDY

In the previous chapters, several investigations were presented: The effect of scatterer/resonator structure on high and low-frequency band gaps, possible ways to refine the structure, and proposals to design the structure according to specific engineering requirements. However, these were all analytical studies. Since errors always exist during finite element analysis, one will not be totally sure whether the results obtained in the simulation can be really achieved in real circumstances. Also, the high attenuations predicted by FEA (e.g. 80-120 dB) are almost never achieved in practice. Therefore, it is necessary to fabricate the structure and test it experimentally.

4.1 MANUFACTURE OF THE STRUCTURE

We will use the structure in Figure 2.4 as the prototype. The finished plate has a finite thickness of 5 mm. Following the procedures listed below and concerning the material parameters in Table 1.1, we have successfully accomplished the manufacturing process.

- The background matrix is made of Somos® ProtoTherm 12120. It is 3D printed by SLA Viper as shown in Figure 4.1. Note that alignment holes for the lead cylinders are printed

in the outer surface. The third surface hole is to inject the silicone rubber around the two lead cylinders.

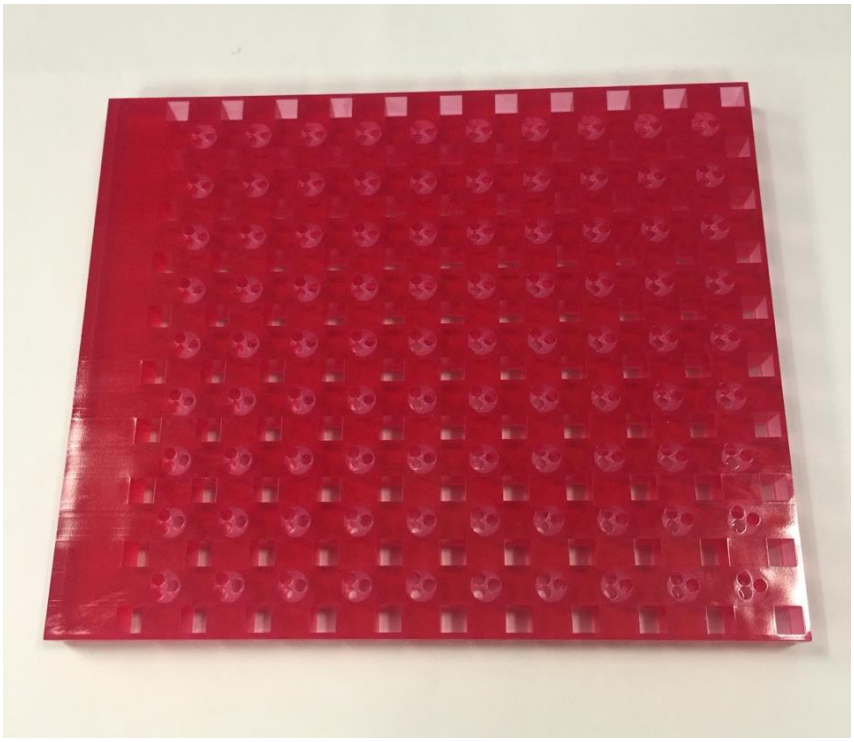

Figure 4.1 Schematic of background matrix

- The GE Ultraglaze SSG4000 is served as our rubber coating
- A lead plate with the dimension of 6’’×6’’ ×1/4’’ was ordered. Then, the plate is cut into several slices with just over 4 mm width each. After that, the lead slices are machined to a thickness of 4 mm and are sawed into small cubes with dimension of 4*4*6 so that the lead square scatterers were obtained. The whole procedure can be summarized by Figure 4.2.

STEP 1:

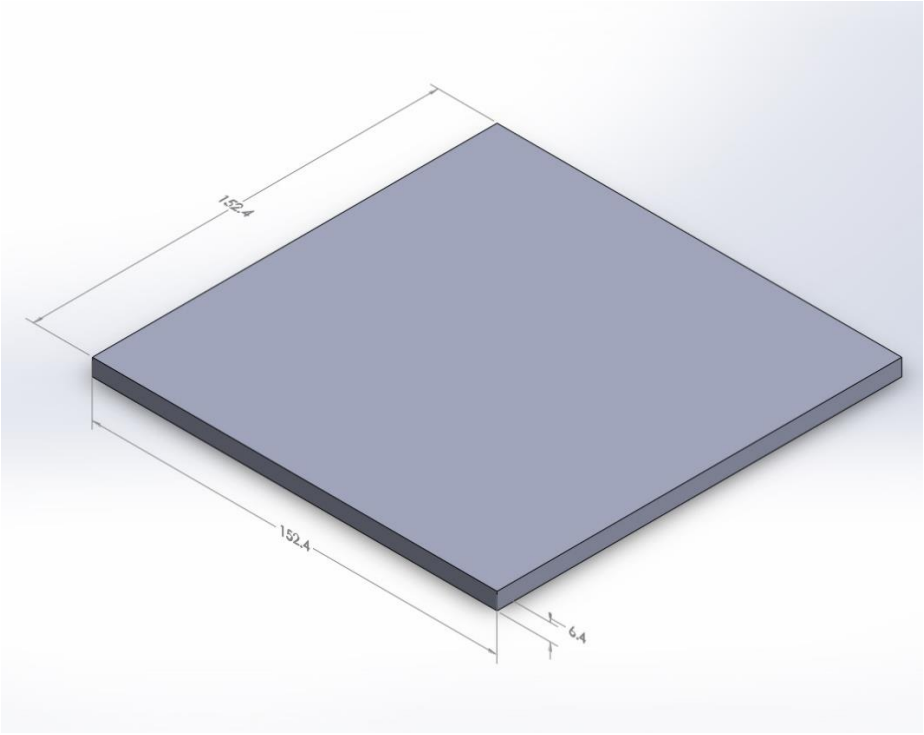

STEP 2:

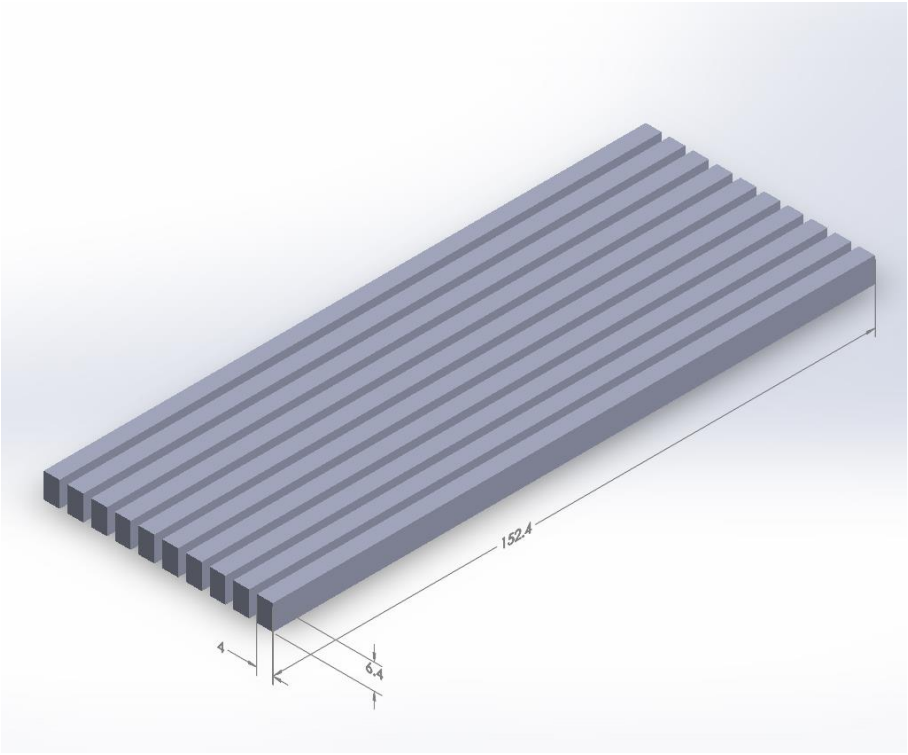

STEP 3:

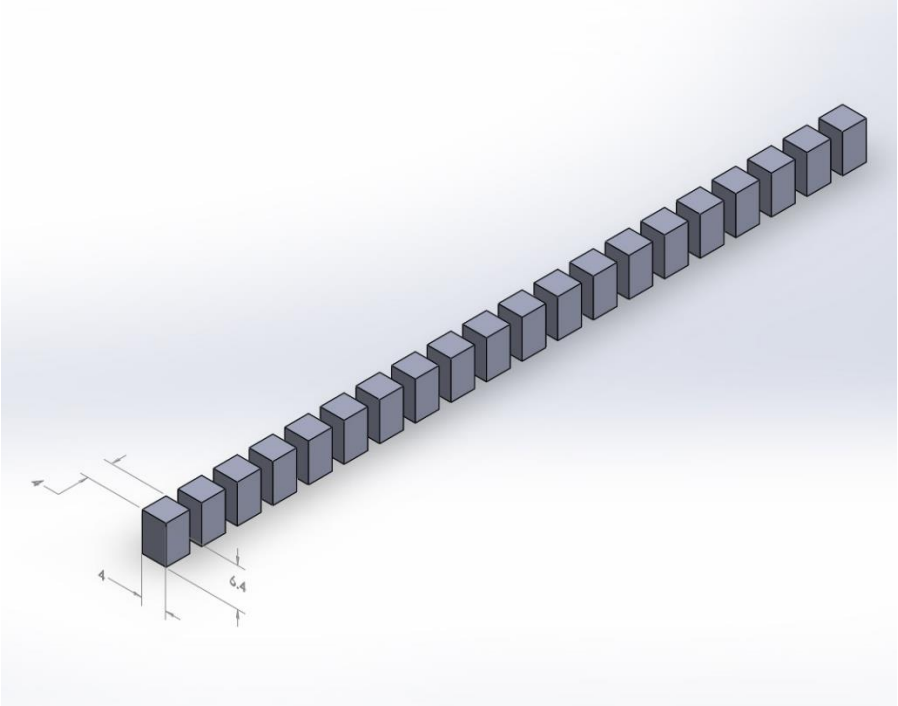

Figure 4.2 Manufacturing procedure for the lead cubes

- Lead wire was ordered and cut into several pieces with length of 6 mm each
- The square lead cubes were glued to Somos ® ProtoTherm 12120 by Locktite Hysol EA 9394 adhesive. Although it is not modeled in this document, according to the material parameters provided by Loctite Inc., compared with the materials that were used during our simulation, a greater mismatch between the epoxy and lead is presented. Therefore, larger gap width and greater vibration attenuation are expected. The lead wire is positioned to the epoxy plate and the wire is surrounded with silicone rubber.
- Once everything is assembled, the upper and lower surfaces are laser cut and the whole structure is machined to a thickness of 5 mm.

The drawing is shown in Appendix A and the whole proposed structure after assembly is shown in Figure 4.2

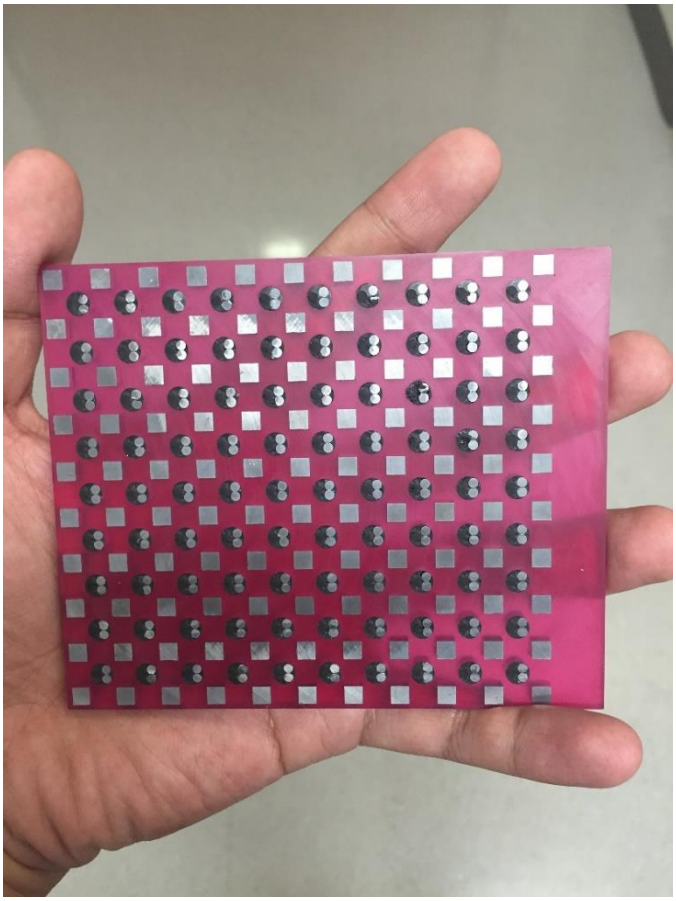

Figure 4.3 The proposed structure after assembling

4.2 EXPERIMENTAL STUDY

The procedure for the entire experiment can be summarized by Figure 4.3 shown below.

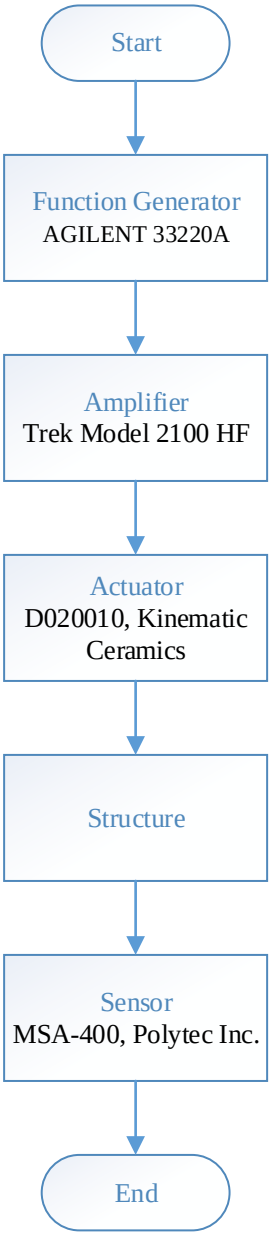

Figure 4.4 Experimental procedure

To begin with, an electric signal is generated by the AGILENT 33220A function generator. This signal is a sine wave with a specific frequency. Then, the electric signal is amplified by 50 times through the amplifier Trek model HF 2100. Thanks to the electric-mechanical coupling effect of the D020010 piezo shacks, the electric signal is then transformed to the mechanical signal,

specifically, the plane wave. After that, the plane wave propagates along the proposed structure and is finally measured by the MSA-400, Polytech Inc. sensor. The data collected in time domain was automatically transformed to frequency domain by Fast Fourier Transformation (FFT). Hence, picking up the peaks in the FFT spectrum allowed us to have the amplitude of the motion under a given frequency. By sweeping the frequency from 0 to 100 kHz, we obtained the output velocity spectrum in frequency domain. The experimental setup is illustrated in Figure 4.4.

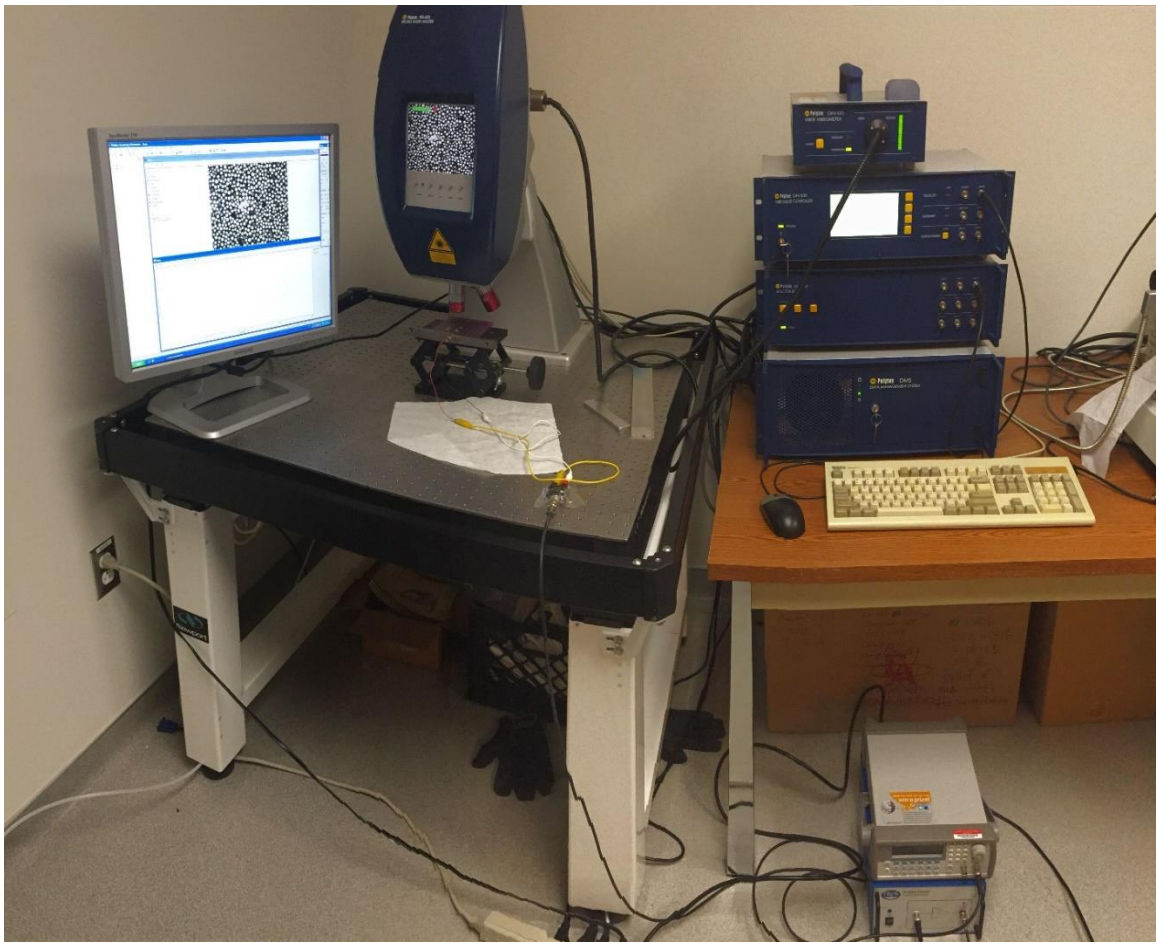

Figure 4.5 Experimental setup

The 5× sensor head is utilized throughout the experiment. Meanwhile, a steel bar is glued between the actuator and the structure. This is for the convenience of generating a plane wave. Unlike the setup in Figure 4.4, the structure is placed vertically at first. However, according to the results, it was found that the structure itself will serve as a vibration absorber. As a result, the wave that was able to propagate to the other end of the structure turned out to be very weak. Thus, when the signal reached the band gap frequency range, it was overwhelmed by noise. Therefore, the structure was oriented in the horizontal direction instead, as shown in Figure 4.5.

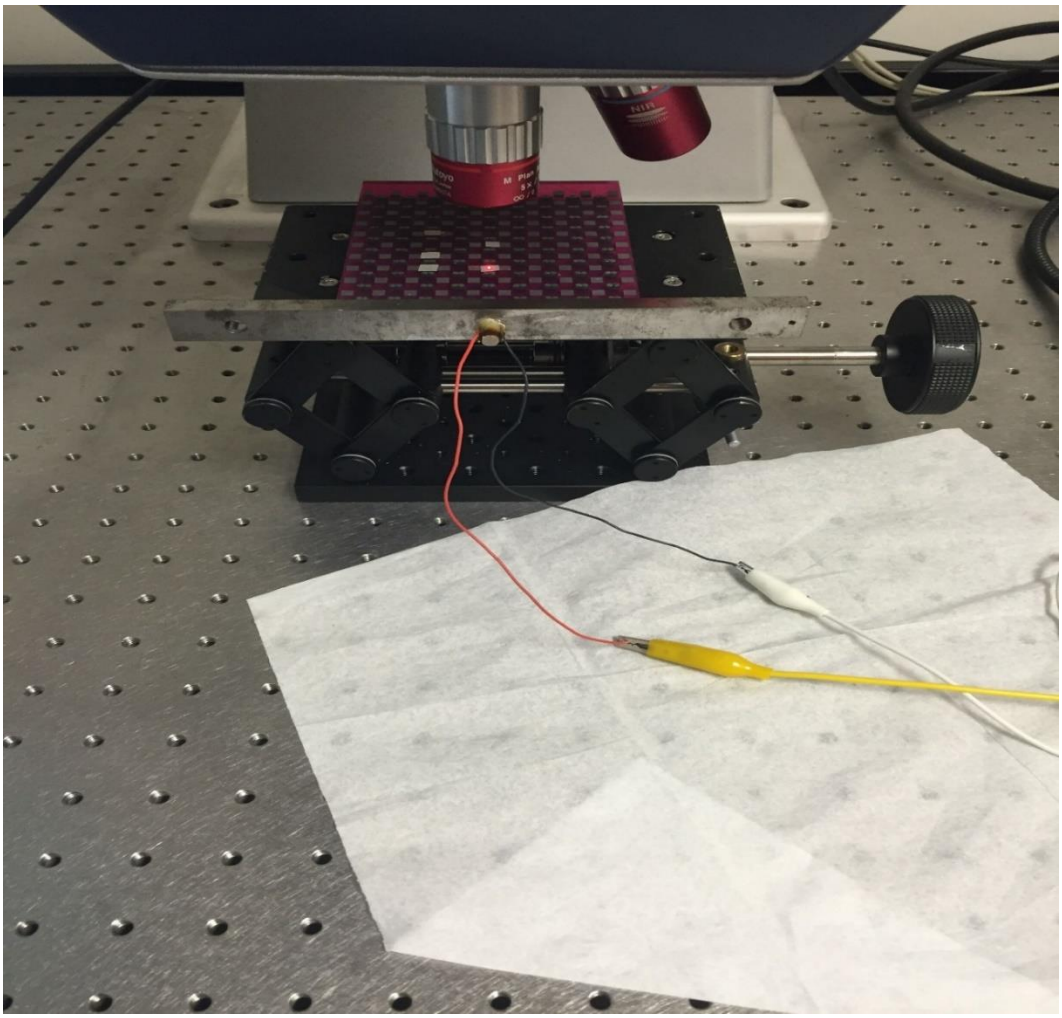

Figure 4.6 Horizontally placed structure

At the same time, we have tested the response at the point which is situated approximately in the middle of the structure. The feasibility of this proposal has been demonstrated in Appendix B. Thanks to the capability of testing the in-plane wave of MSA-400, Polytech Inc., the experiment turned out to be a success. The output velocity is plotted in Figure 4.6. Several discrete frequencies were measured by manually sweeping the frequency on the function generator and measuring the response.

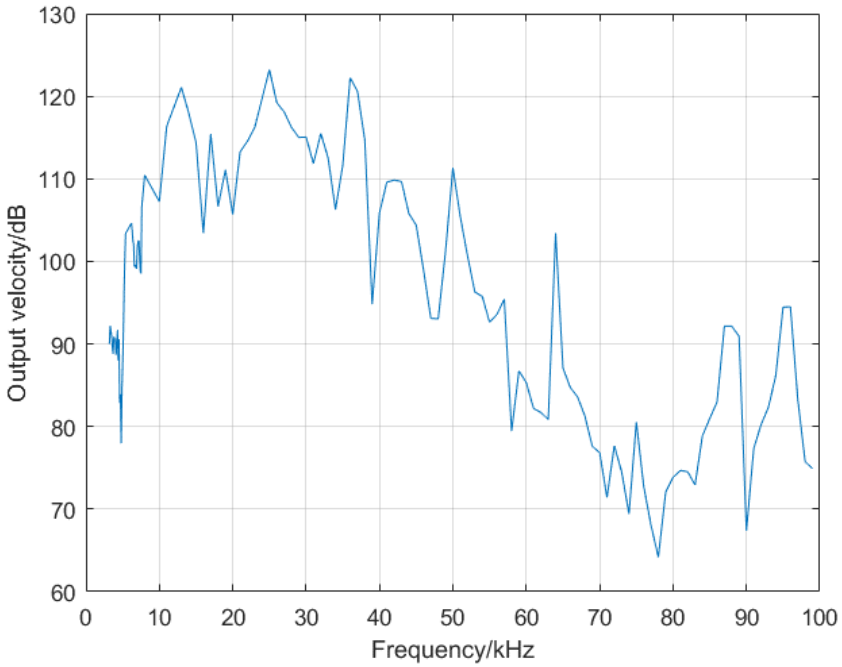

Figure 4.7 Output velocity of the structure

The output velocity is transformed into a vibration level by the following equation[42]

$$L_v = 20log_{10}\frac{v}{v_0} \tag{4-1}$$

where v_0 is an internationally accepted reference value of

$$v_0 = 10^{-9}\text{m s}^{-1} \tag{4-2}$$

It is quite clear that in the lower frequency range, especially at the frequency of 4800 Hz, the velocity obtained is at a minimum. In the meantime, in the higher frequency range, especially the frequency range of 70-90 kHz, another band gap appears. However, it is easy to find out in Figure 4.5 that, unlike the simulation where the transmission spectrum is oscillating about a constant, the overall spectrum is first increased and then decreased. This is affected by the input signal. Therefore, to eliminate the effects and to meet our simulation, we have tested the transmission of the structure. Before that, it is necessary to determine the motion of the actuator. This is accomplished by inverting the structure as shown in Figure 4.7.

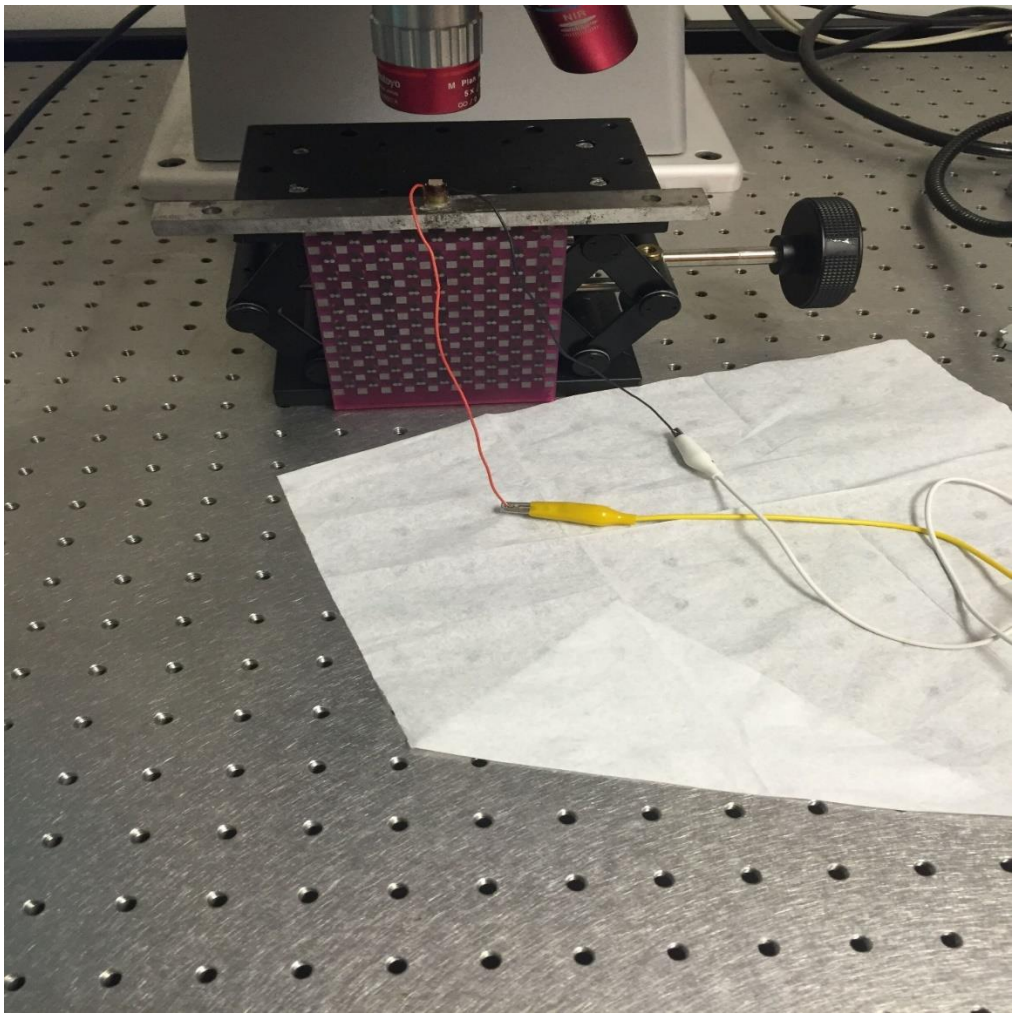

Figure 4.8 Schematic of the structrue after flipping over

The corresponding response of the actuator is illustrated in Figure 4.8

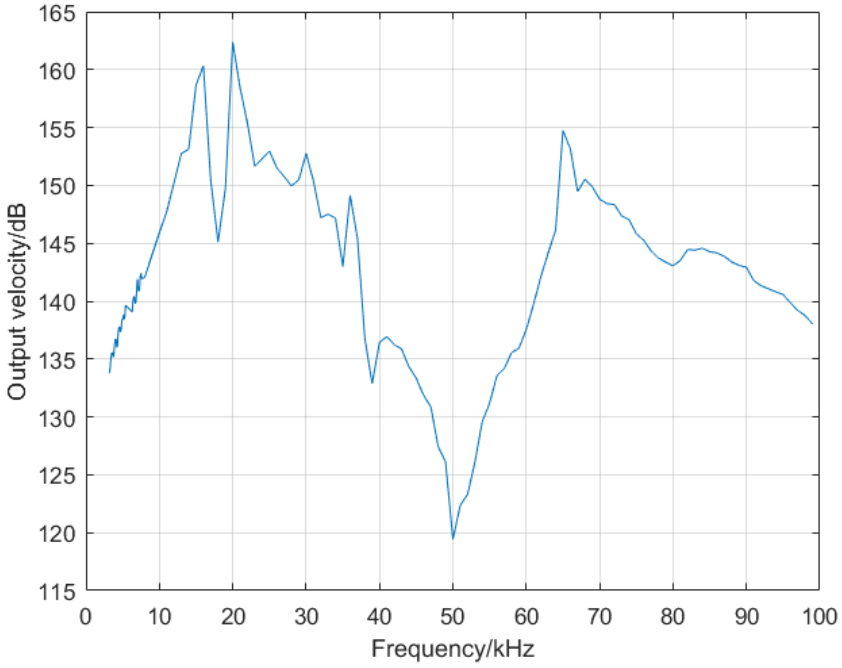

Figure 4.9 Motion of the actuator

From Figure 4.8, it is quite clear that during the entire frequency range, three main peaks appear which will correspond to the resonance of the piezo shacks. Having this in mind, we can come up with the transmission spectrum according to Eqn. (1-11). The experimental transmission spectrum is illustrated in Figure 4.9.

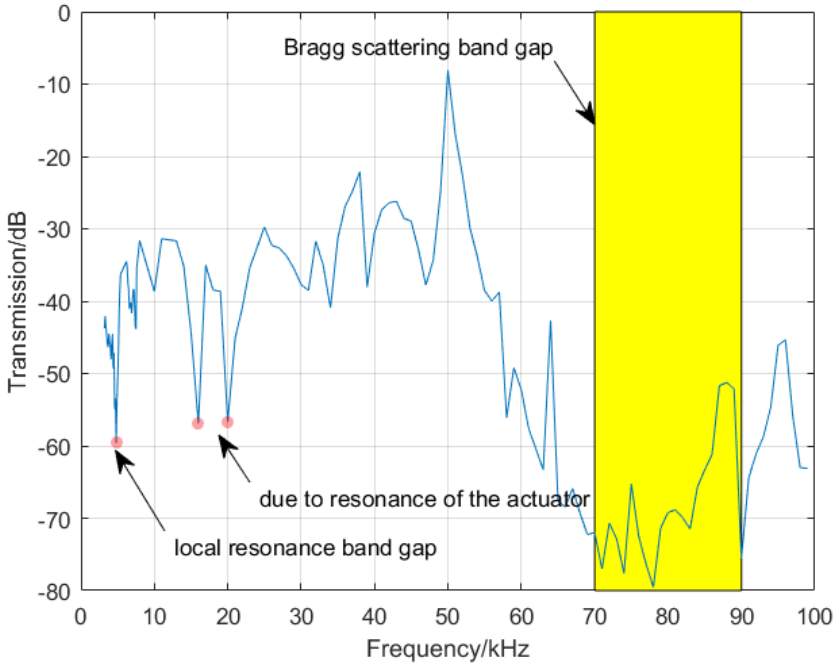

Figure 4.10 Transmission spectrum of the proposed structure from input to mid-structure

As illuminated by Figure 4.9, in the lower frequency range, there is a 60 dB vibration attenuation at 4800 Hz. However, at this time, there are other peaks at 16 kHz and 20 kHz which are due to the resonance of the actuator. They will disappear when other type of actuators are utilized. In the meantime, in the frequency range of 70 kHz to 90 kHz, a maximum of approximately 40 dB vibration attenuation is obtained. Although the exact value of vibration attenuation is not exactly the same as the simulation which has been explained in Appendix B, these experimental results coincide with our simulation quite well. We are able to find a gap at 4800 Hz. It is due to the local resonance of the double lead core and the soft rubber coating. At the frequency range of 65-95 kHz, another band gap is obtained as a result of Bragg scattering among lead cubes.

5.0 CONCLUSION AND OUTLOOK

In this document, a novel two dimensional acoustic metamaterial with Coated Double Hybrid Lattice (CDHL) is presented. Both the simulations and experiments have illustrated the effectiveness of the proposed structure.

Traditional finite element analysis was used to simulate this and other structures. Both a lower frequency band gap and a higher frequency band gap are obtained. The lower frequency band gap appears because a local resonance between double lead cores and rubber coating takes place. By carrying out both modal analysis and phase spectrum analysis, it is demonstrated that the higher frequency band gap is a result of the interaction of local resonances and Bragg scattering. To optimize the whole structure, the relationship between vibration attenuation and the position of the double circular scatterers is summarized. An order of magnitude more attenuation in vibration attenuation is predicted in the end.

In the experimental study, the wave is generated by a piezo shack and is measured by MSA-400, Polytech Inc. Both the lower frequency band gap and the higher frequency band gap are obtained. Despite the fact that the amount of vibration attenuation is not exactly the same as the simulation, the band gap position coincides quite well with the simulation.

Since there is always room for further improvement of the experiments, the author will suggest the following future work. First of all, a piezo shack with greater displacement can be used as an actuator so that it is easier to pick up signals on the output. As a result, the vibration

attenuation of the entire proposed structure can be visualized, since the response will be well above the noise floor. Second, better ways of supporting the structure should be considered. For example, one may consider supporting the structure by two parallel clamps and finding proper screws to fix the clamps to the isolation table. This will further isolate the possible noise and refine the results.

APPENDIX A

DRAWING OF THE WHOLE STRUCTURE

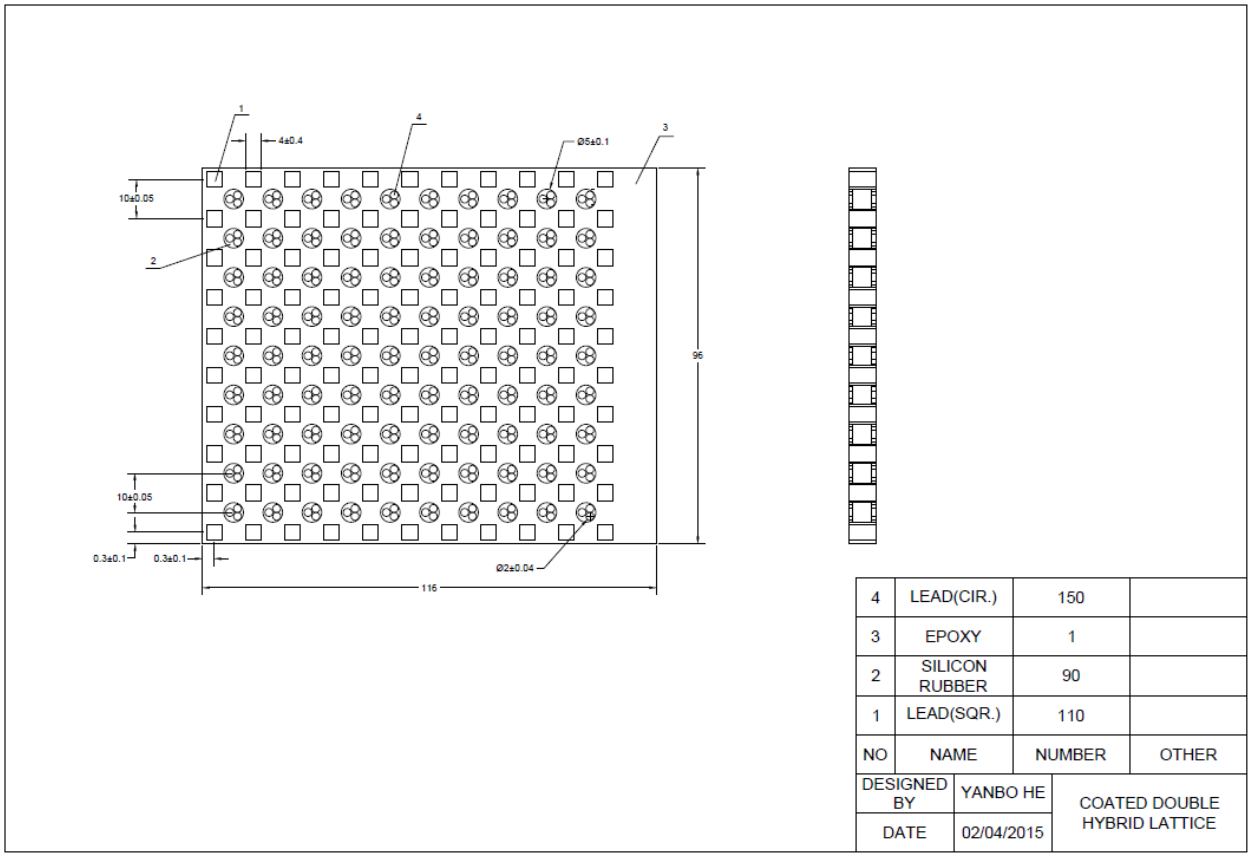

4	LEAD(CIR.)	150	
3	EPOXY	1	
2	SILICON RUBBER	90	
1	LEAD(SQR.)	110	
NO	NAME	NUMBER	OTHER

DESIGNED BY	YANBO HE	COATED DOUBLE HYBRID LATTICE
DATE	02/04/2015	

Figure A.1 Drawing of the proposed structure

APPENDIX B

VALIDATION OF PICKING UP SIGNALS AT MIDDLE OF THE STRUCTURE

In the experiments, instead of picking up signals at other end of the structure, we tested the output velocity in the middle of the structure. This is different from our simulation but it is still valid. Therefore, this section is intended to validate the feasibility of the experimental method via finite element analysis. To begin with, the original displacement field is plotted in Figure B.1. In this case, the maximum displacement is set to be 1 m.

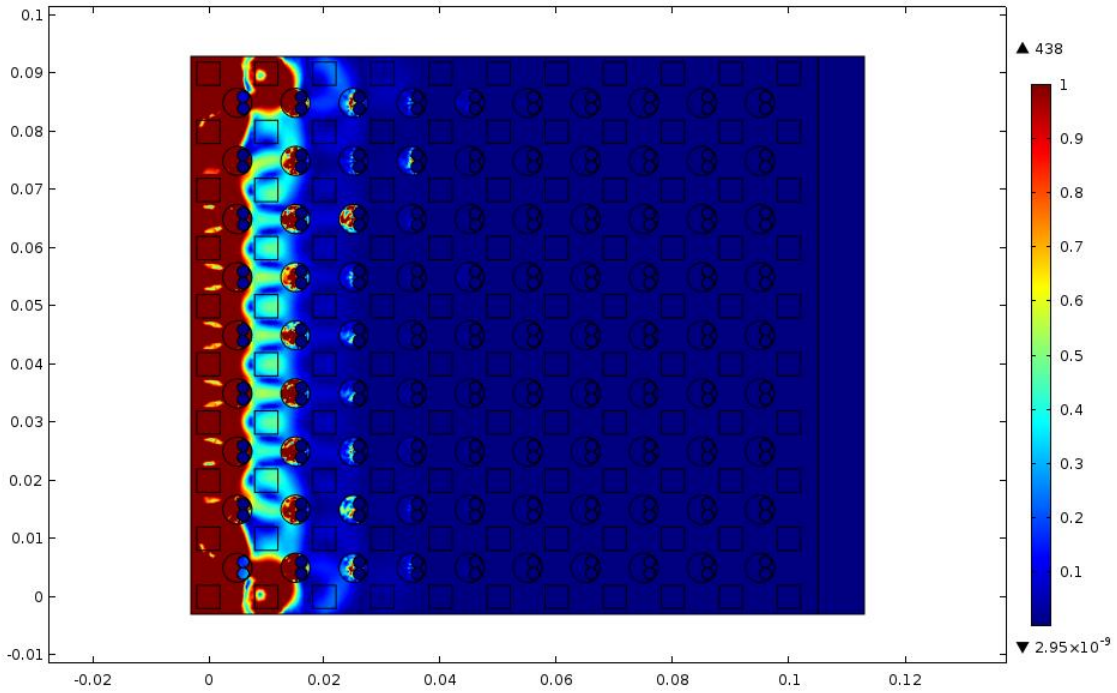

Figure B.1 Displacement field with the maximum displayable displacement of 1 m

In the later Figures, we will pick the same displacement field with the same frequency but will lower the maximum displacement that is displayed.

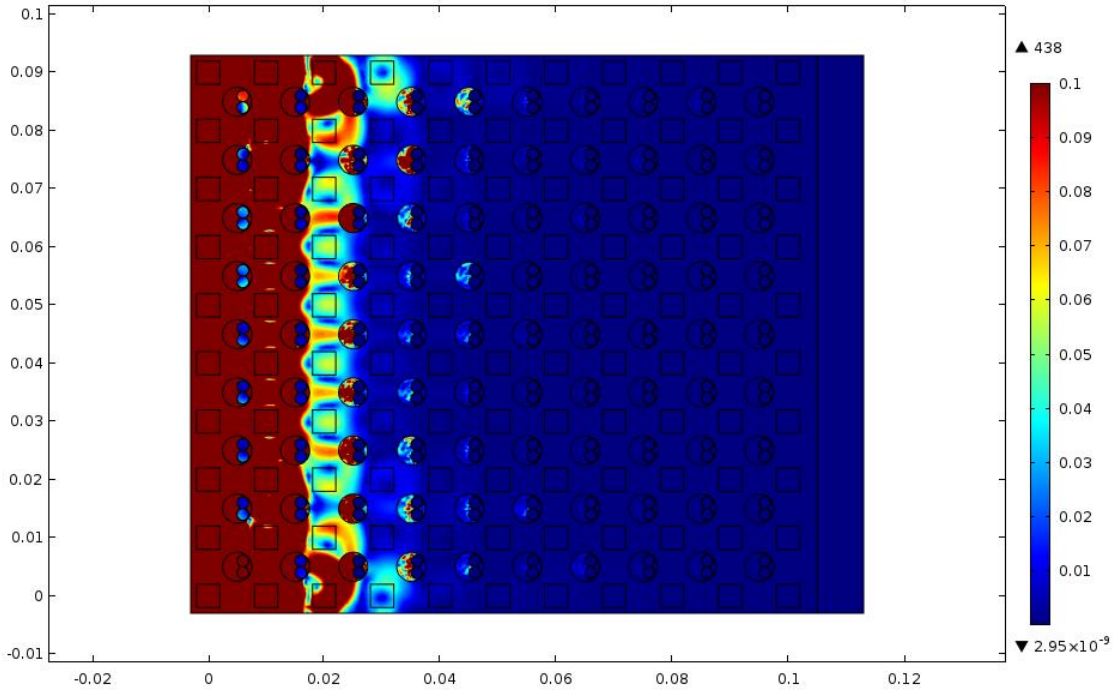

Figure B.2 Displacement field with the maximum displayable displacement of 0.1 m

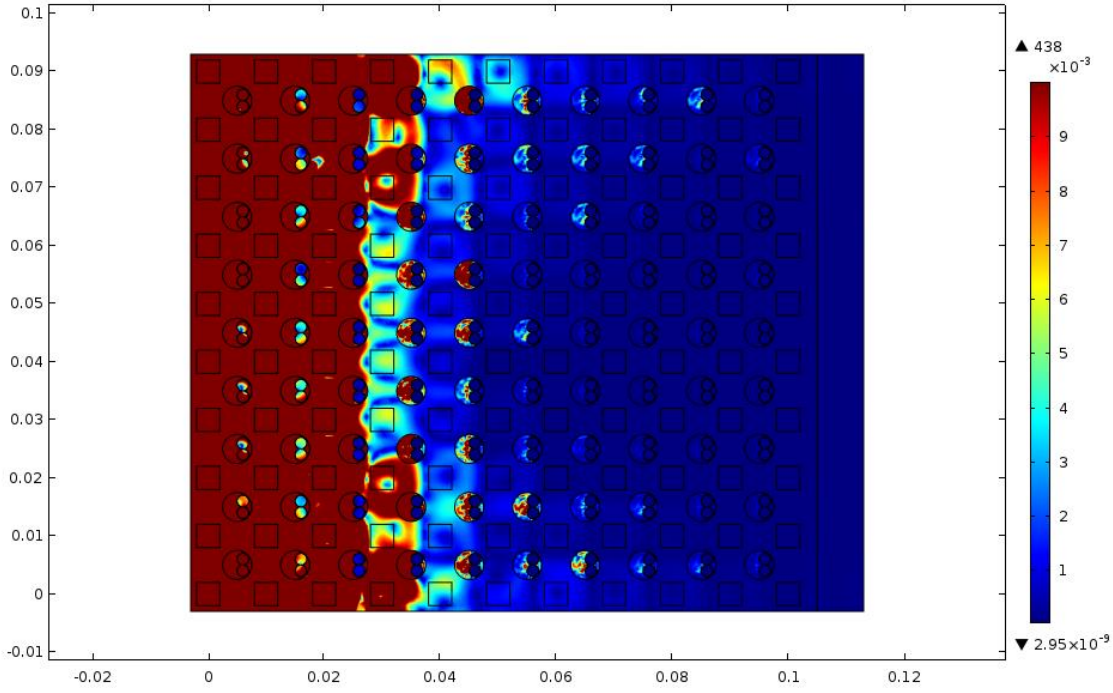

Figure B.3 Displacement field with the maximum displayable of 0.01 m

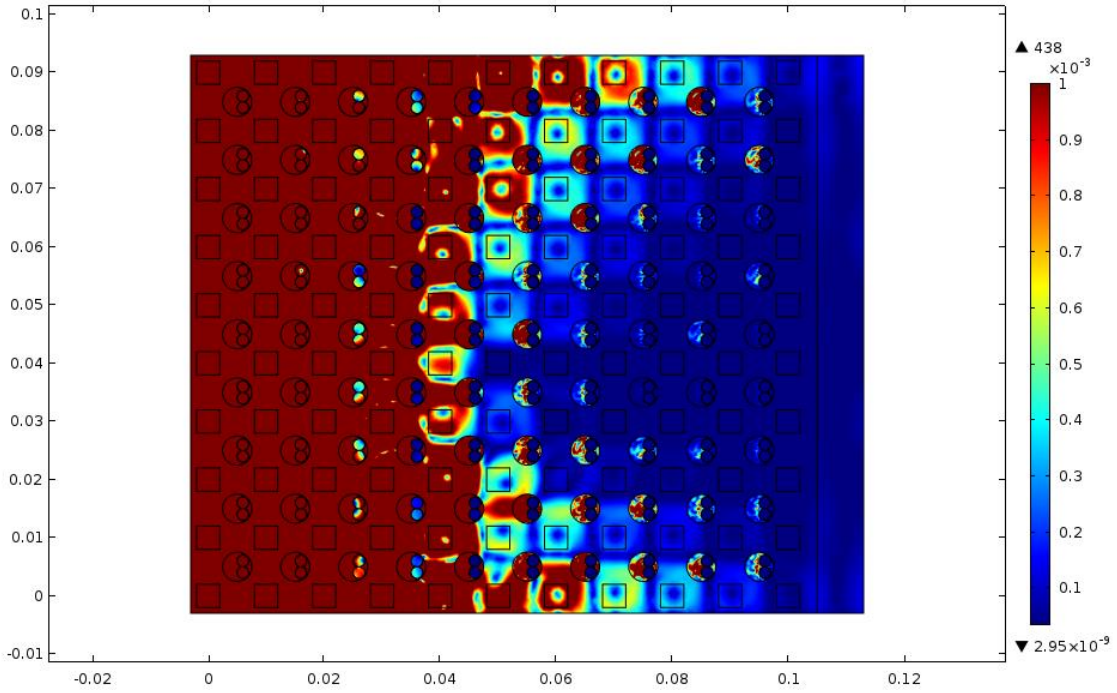

Figure B.4 Displacement field with the maximum displayable of 0.001 m

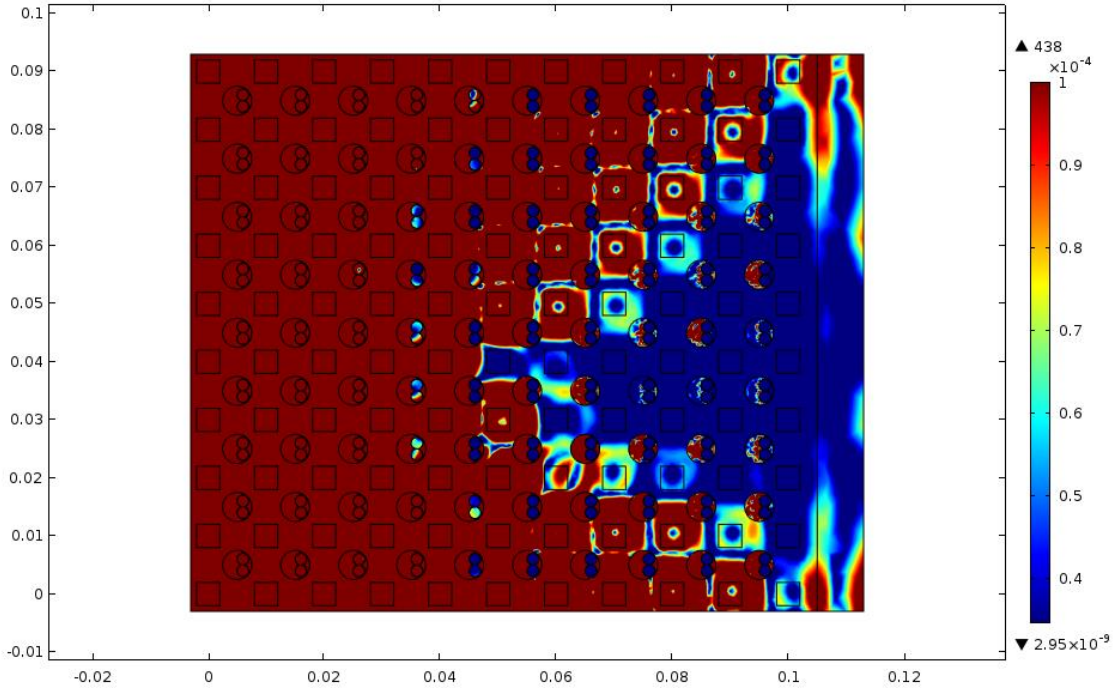

Figure B.5 Displacement field with the maximum displayable of 1×10-4 m

Figure B.2 to Figure B.5 illustrated the variation of the displacement field at the same frequency, but with varying maximum displacement scales that range from 0.1 m down to 1×10^{-4} m. It is quite clear that the wave is attenuated with each successive unit cell. The vibration attenuation will reach a maximum at the other end of the structure. Therefore, the most optimized situation is to pick up the signal at the other end since this will obtain not only the correct band gap position but also the right vibration attenuation. However, as stated in Chapter 4, due to the fact that it is hard to pick up signals at the other end with the current actuators due to high signal to noise ratio. We decided to test the velocity in the middle of the structure. Although it is different from our simulation, it is still feasible, that is, we may sacrifice some vibration attenuation but still can get the correct structure of the transmission spectrum and band gap.

APPENDIX C

VALIDATION OF PHASE SPECTRUM CALCULATION

As indicated in section 1.1.3, the proposed structure in this document is intended to make use of both the local resonance theorem and the Bragg scattering theorem. However, there are cases where a local resonance derived gap may interfere with a Bragg scattering band gap. Hence, it is necessary to understand the formation of the band gap and identify one gap from another. Therefore, the phase calculation put forward by Elford is utilized here to identify a local resonant derived gap from a Bragg scattering derived gap[39].

In order to only transmit longitudinal waves, we will place the structure in water. Waves are excited or measured in water on either side of the structure (shown in fig C.1). The phase is computed between the input location and either points A or B in the water at the front or back of the structure, respectively.

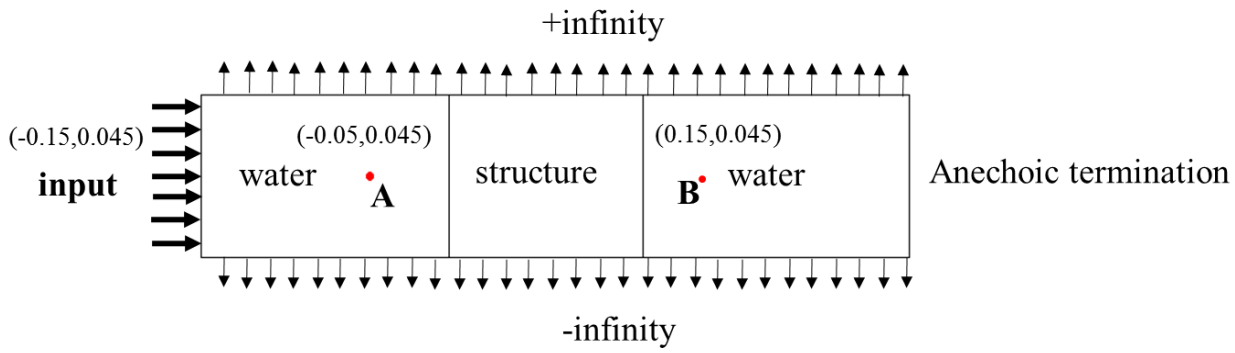

Figure C.1 Schematic of structure in water

The uniformly distributed incident wave with amplitude of 1 Pa on the left boundary is denoted as

$$p = 1 * e^{-\mathrm{i}kx} = \cos(kx) - \mathrm{i} * \sin(kx) \quad \text{(C-12)}$$

where k is the wave number and x, in this specific case, denotes the position of the incident wave, that is, x=-0.15. Then, the real part and imaginary part of the incident wave should be in the form of cosine and sine wave respectively.

$$\mathrm{real}(p) = cos(0.15k) \quad \text{(C-13)}$$

$$\mathrm{imag}(p) = sin(0.15k) \quad \text{(C-14)}$$

These equations correspond to the Figure C.2 and Figure C.3 respectively

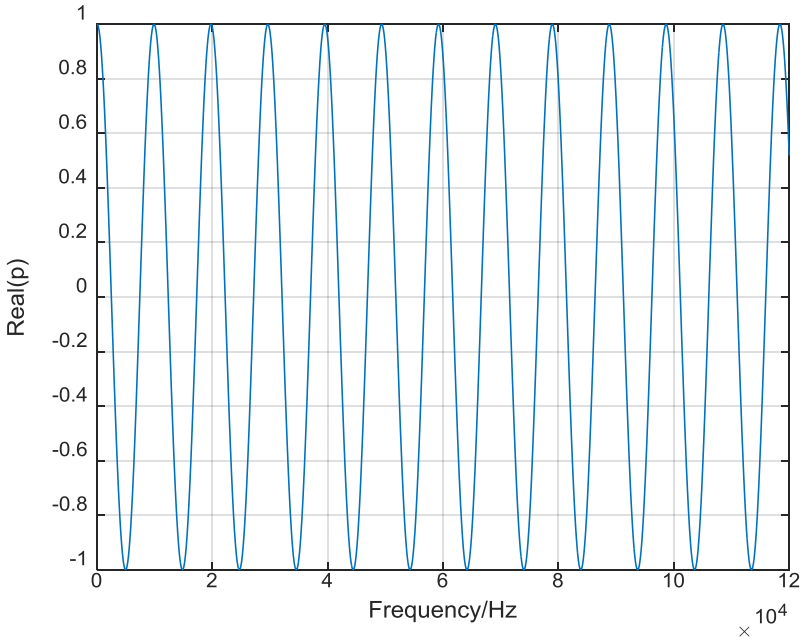

Figure C.2 Real part of incident wave

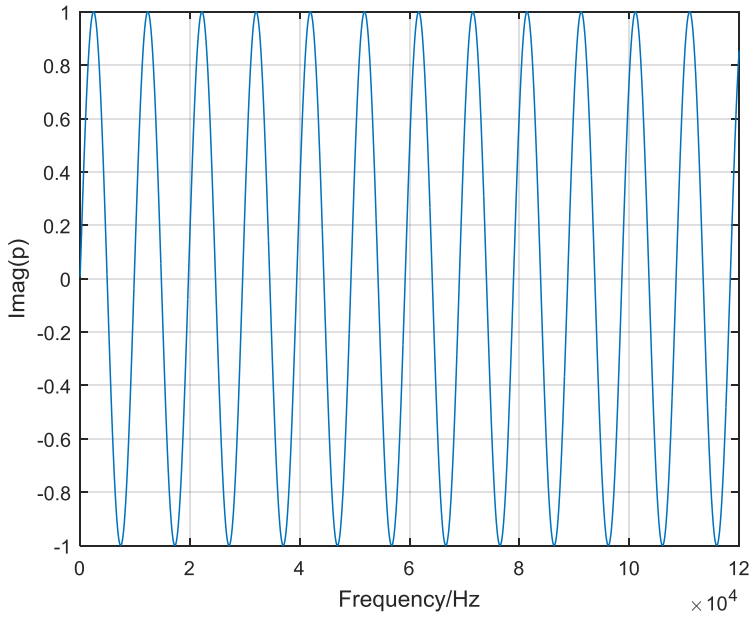

Figure C.3 Imaginary part of incident wave

Moreover, the upper and lower boundaries are set as Bloch periodic conditions as stated by eqn. (1-8). For the pure structure with no scatterers, it is equivalent to a boundary condition where no reflection will occur. The simulated test environment is demonstrated by Figure C.4.

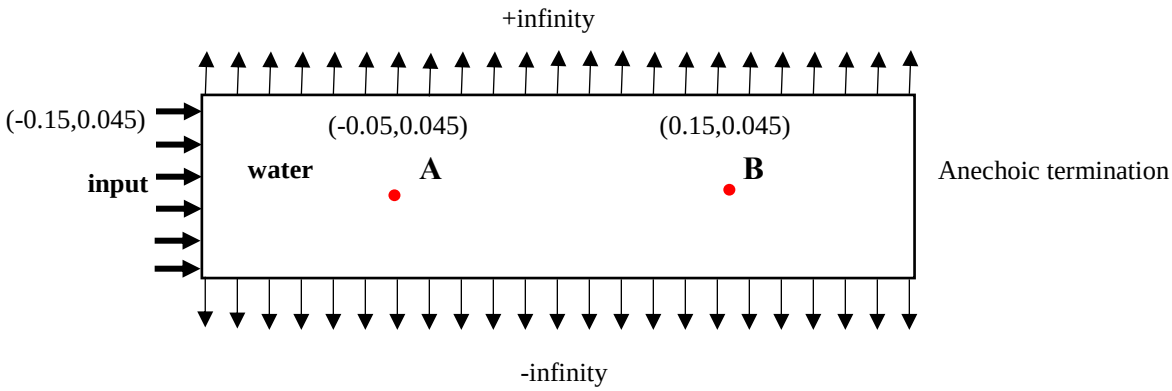

Figure C.4 Schematic of the simulated test environment with pure water

Meanwhile, the back side is set to the plane wave radiation boundary condition which is to guarantee that no reflection will take place from the back side as well.

We will start with the simplest case where there is only water in the system. In this case, it is quite easy to come up with the corresponding phase, that is,

$$\varphi = -kx \tag{C-15}$$

where k is the wave number expressed as

$$k = \frac{2\pi f}{c} \tag{C-16}$$

in which f the frequency and c is the wave speed of the water. Hence, if there is only one material, no reflection exists in the system, we can write the phase taken at the input boundary, point A and point B respectively as

$$\varphi_i = 0.15 * k \tag{C-17}$$

$$\varphi_A = 0.05 * k \tag{C-18}$$

$$\varphi_B = -0.15 * k \tag{C-19}$$

To better illustrate how the phase taken at point A and point B will vary with respect to the input phase, a relative phase is introduced as

$$\varphi_r = \varphi_{A/B} - \varphi_i \tag{C-20}$$

and the phase taken at point A and B with respect to the input phase can be further derived as

$$\varphi_1 = -0.1 * k \tag{C-21}$$

$$\varphi_2 = -0.3 * k \tag{C-22}$$

The corresponding phase spectrum can be plotted in Figure C.5 and Figure C.6. Since in this case, all the boundaries are set as reflection-free, either the relative phase taken at front point A or back point B will represent a linearly decreasing spectrum which is the case represented by Figure C.5 and Figure C.6.

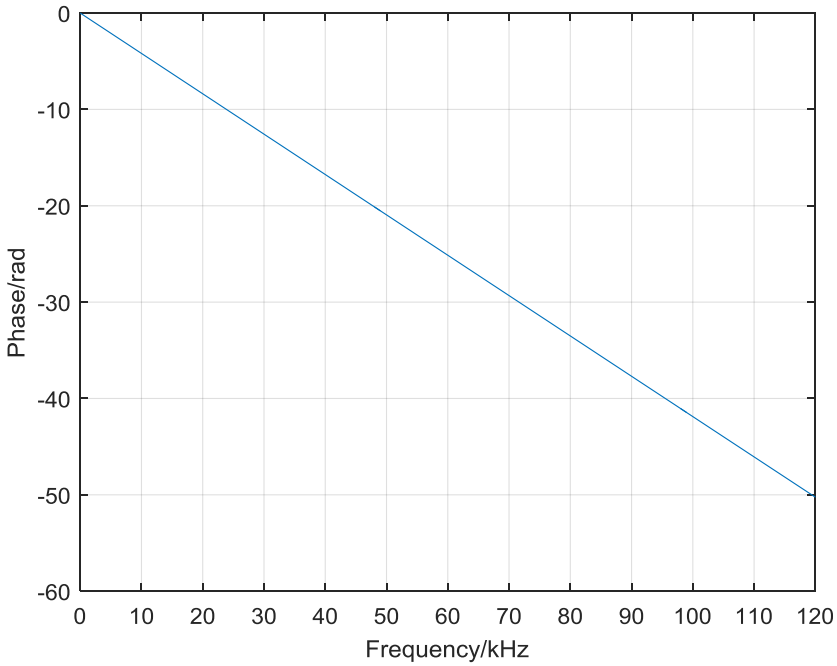

Figure C.5 Relative phase spectrum taken at point A of pure water system

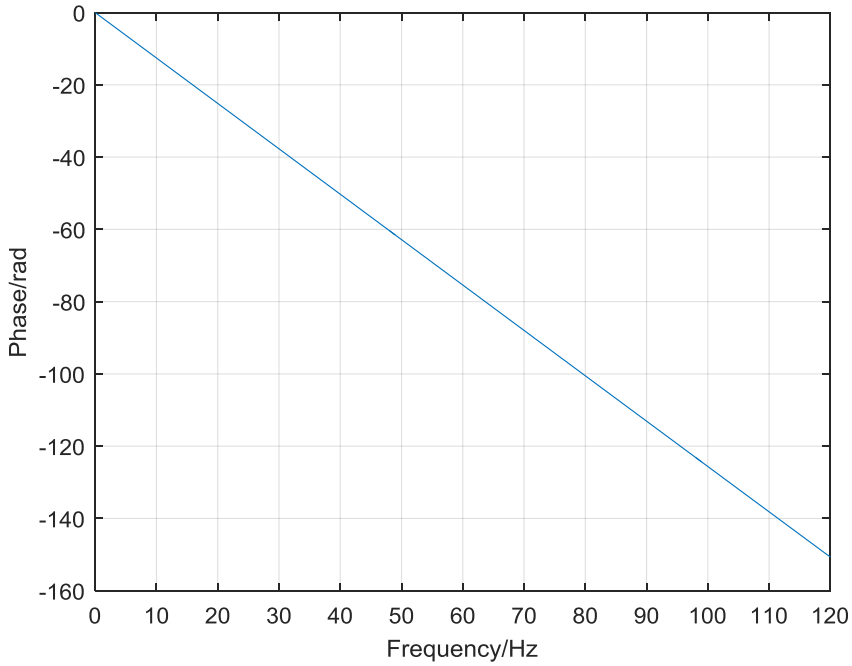

Figure C.6 Relative phase spectrum taken at point B of pure water system

After the discussion of pure water structure, we continued to investigate the case where an epoxy plate was placed in the water with the same boundary conditions. The schematic of the system is plotted in Figure C.7

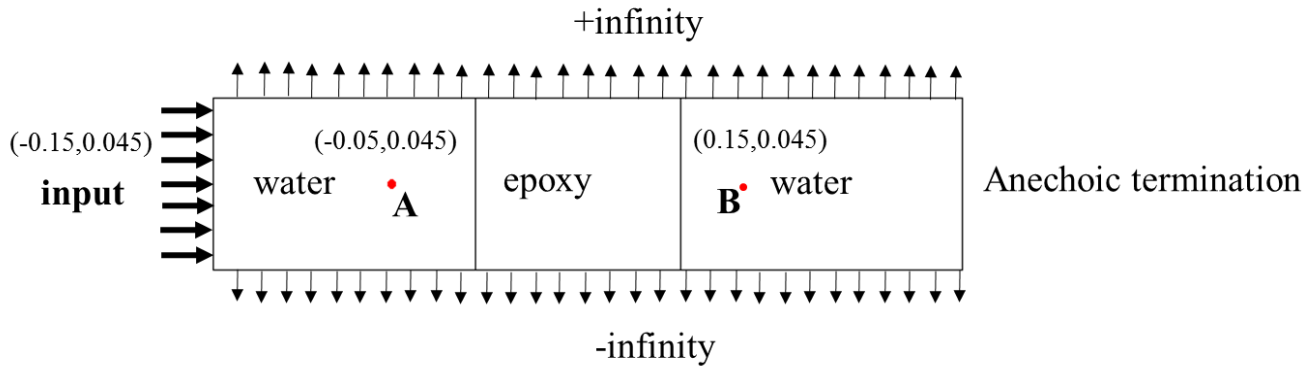

Figure C.7 Schematic of epoxy plate in water

Following the same procedure, we have come up with the relative phase spectrum which is plotted in Figure C.8 and Figure C.9.

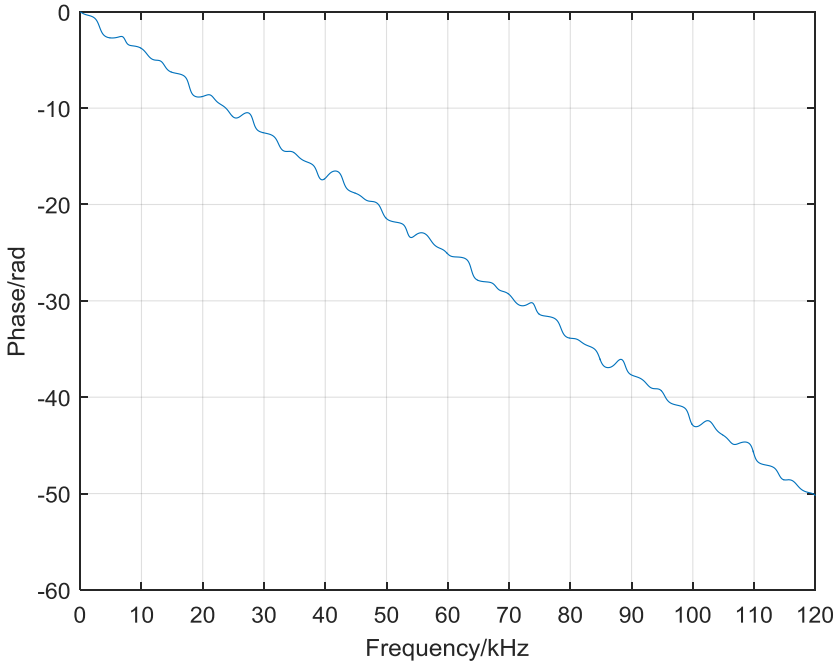

Figure C.8 Relative phase spectrum taken at point A of epoxy-water system

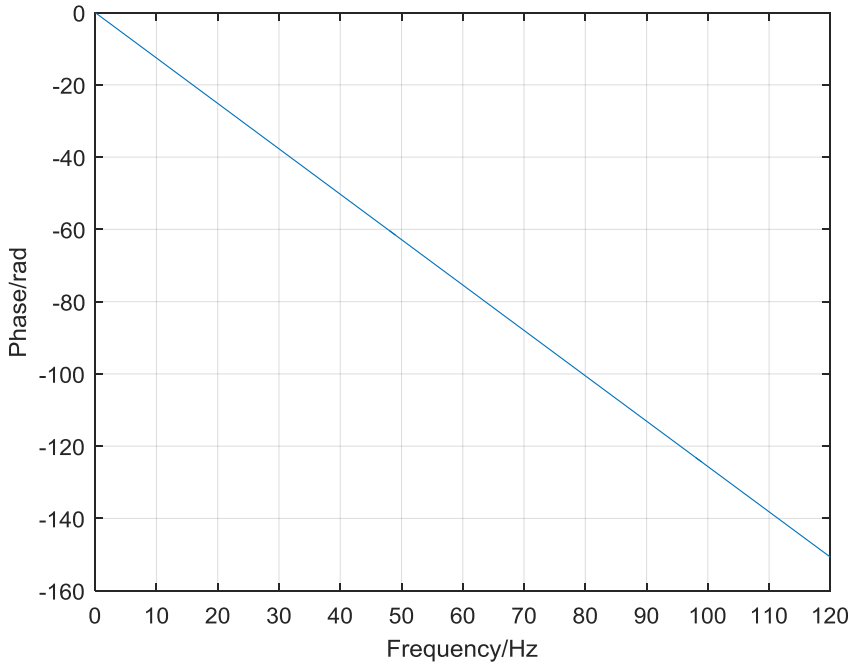

Figure C.9 Relative phase spectrum taken at point B of epoxy-water system

Similarly, either the relative phase taken at the front point A or the back point B gives us a monotonically decreased spectrum. However, quite different from the pure water system, there are several oscillations in the diagram. Obviously, these oscillations will have nothing to do with the boundary effects since the top, bottom and back side boundaries are all set to be anechoic. Therefore, these oscillations are believed to be a result of the reflection on the solid-fluid boundary of the system. Keeping this in mind, a more comprehensive structure is introduced, the schematic of which is shown in Figure C.10.

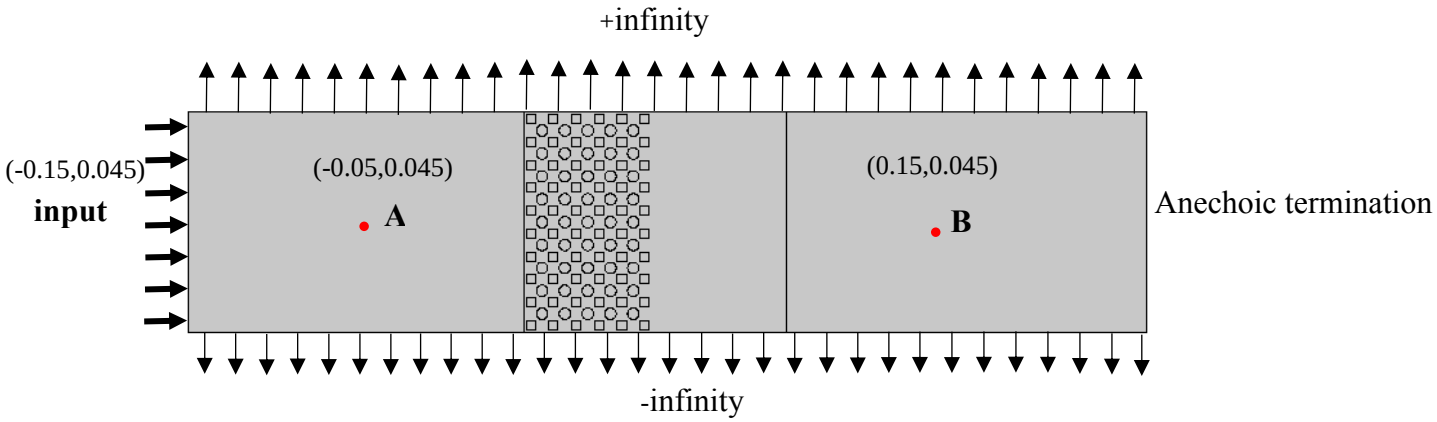

Figure C.10 Schematic of half lead-epoxy structure in water

This time, an epoxy matrix half filled with hybrid lead squares and circle scatterers is fabricated. This is an ordinary case where the band gap will appear in the range of 80 kHz-120 kHz. To test Elford's conclusion, we have plotted the relative phase spectrum taken at the front point A and back point B which are presented in Figure C.11 and Figure C.12 respectively.

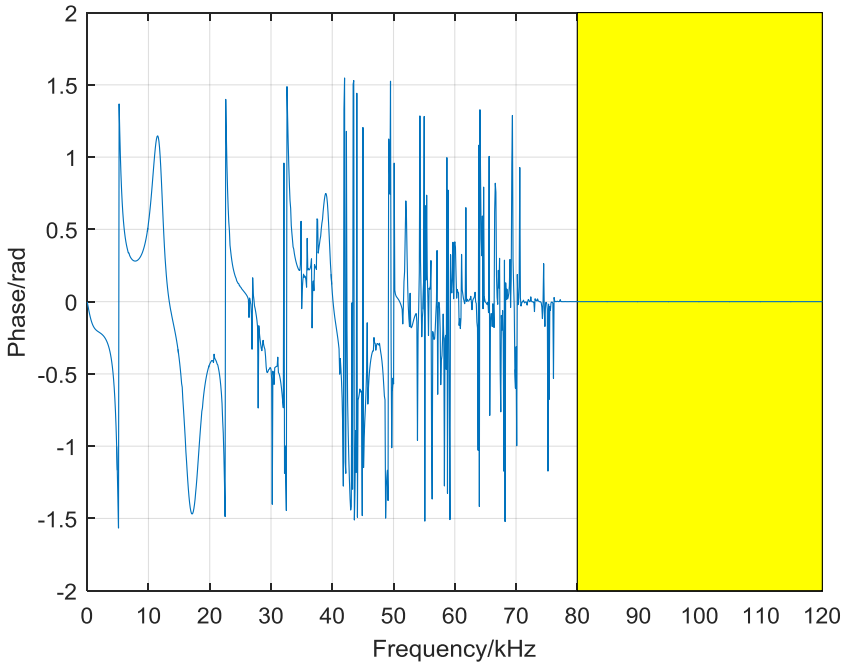

Figure C.11 Relative phase spectrum taken at point A of half lead-epoxy-water system

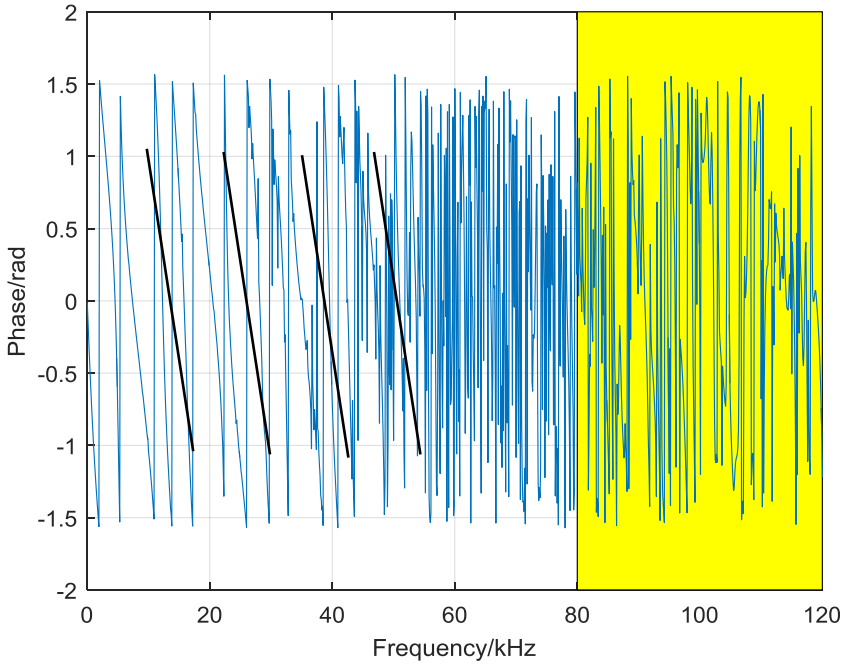

Figure C.12 Relative phase spectrum taken at point B of half lead-epoxy-water system

According to Elford's conclusion, if a Bragg scattering derived band gap is obtained within a specific frequency range, the relative phase taken at the front should keep a constant whereas the phase taken at the back should no longer oscillate between $+\pi$ and $-\pi$[39]. By looking into Figure C.11 and Figure C.12, it is clear that, generally speaking, the relative phase is still decreasing. However, quite many peaks appear in the spectrum and these peaks correspond to possible reflections from the many solid-solid and solid-fluid boundaries. In the meantime, in the frequency range of 7.5-12 kHz, the phase taken at the front point A (not shown) remains constant, whereas the phase taken at the back point B no longer linearly decreases, but rather, oscillates between $+\pi/2$ and $-\pi/2$. In fact, these results have met the conclusion that has been summarized by Elford, that is, if there is no scattering in a frequency range, a linear phase response will be observed at both measurement points, corresponding to the propagation delay between the input position and respective measurement point[39]. However, where there is wave scattering, the phase taken before the structure (pt. A) will remain a constant, whereas the phase spectrum taken after the structure (pt. B) is no longer linearly decreasing.

BIBLIOGRAPHY

1. Deymier, Pierre A., ed. *Acoustic metamaterials and phononic crystals*. Vol. 173. Springer Science & Business Media, 2013.

2. Sigalas, M., and E. N. Economou. "Band structure of elastic waves in two dimensional systems." Solid State Communications 86.3 (1993): 141-143.

3. Kushwaha, Manvir S., et al. "Acoustic band structure of periodic elastic composites." Physical Review Letters 71.13 (1993): 2022.

4. R. Martinez-Sala, J. Sancho, J.V. Sanchez, et al. Sound attenuation by sculpture[J]. Nature, 1995, 378(1): 241-248.

5. Huang, H. H., and C. T. Sun. "Wave attenuation mechanism in an acoustic metamaterial with negative effective mass density." New Journal of Physics, 11.1 (2009): 013003.

6. Sun, Jia-Hong, and Tsung-Tsong Wu. "Propagation of acoustic waves in phononic-crystal plates and waveguides using a finite-difference time-domain method." Physical Review B 76.10 (2007): 104304.

7. Zhu, Hongfei, and Fabio Semperlotti. "Metamaterial based embedded acoustic filters for structural applications." AIP Advances 3.9 (2013): 092121.

8. Yang, Wen-Pei, and Lien-Wen Chen. "The tunable acoustic band gaps of two-dimensional phononic crystals with a dielectric elastomer cylindrical actuator." Smart Materials and Structures 17.1 (2008): 015011.

9. Brillouin, Léon. Wave propagation in periodic structures: electric filters and crystal lattices. Courier Corporation, 2003.

10. Ming-Hui Lu, Liang Feng, and Yan-Feng Chen. "Phononic crystals and acoustic metamaterials." Materials Today 12.12 (2009): 34-42.

11. Xiao-Zhou Zhou, Yue-Sheng Wang, and Chuanzeng Zhang. "Effects of material parameters on elastic band gaps of two-dimensional solid phononic crystals." Journal of Applied Physics 106.1 (2009): 014903.

12 Tian-Xue Ma, et al. "Effects of material parameters on elastic band gaps of three-dimensional solid phononic crystals." Physica Scripta 87.5 (2013): 055604.

13 Vicente Romero-García,, et al. "Multi-resonant scatterers in sonic crystals: Locally multi-resonant acoustic metamaterial." Journal of Sound and Vibration 332.1 (2013): 184-198.

14 Weimin Kuang, Zhilin Hou, and Youyan Liu. "The effects of shapes and symmetries of scatterers on the phononic band gap in 2D phononic crystals." Physics Letters A 332.5 (2004): 481-490.

15 Vicente Romero-García, et al. "Multi-resonant scatterers in sonic crystals: Locally multi-resonant acoustic metamaterial." Journal of Sound and Vibration 332.1 (2013): 184-198.

16 Graciá-Salgado Rogelio, Daniel Torrent, and José Sánchez-Dehesa. "Double-negative acoustic metamaterials based on quasi-two-dimensional fluid-like shells." New Journal of Physics 14.10 (2012): 103052.

17 Sz-Chin Steven Lin, and Tony Jun Huang. "Tunable phononic crystals with anisotropic inclusions." Physical Review B 83.17 (2011): 174303.

18 Xiujuan Zhang, and Ying Wu. "Effective medium theory for anisotropic metamaterials." Scientific reports 5 (2015).

19 Yanyu Chen and Lifeng Wang. "Periodic co-continuous acoustic metamaterials with overlapping locally resonant and Bragg band gaps." Applied Physics Letters 105.19 (2014): 191907.

20 Jingtao, Du, Yanbo He and Haocheng Feng. “Effects of the rotation angle of scatterers on the band gap structure of a two-dimensional phononic crystal” Harbin Gongcheng Daxue Xuebao/Journal of Harbin Engineering University, 35.11 (2014), p 1358-1363

21 Y. W. Yao, Z. L. Hou, Y. Y. Liu, The two-dimensional phononic band gaps tuned by the position of the additional rod [J]. Physics Letters A, 362, (2007) 494-499

22 Aravantinos-Zafiris, N., and M. M. Sigalas. "Large scale phononic metamaterials for seismic isolation." Journal of Applied Physics 118.6 (2015): 064901.

23 Zhengyou Liu, et al. "Locally resonant sonic materials." Science 289.5485 (2000): 1734-1736.

24. L.X. Li, T.N. Chen, J.H. Wu, and Xiaopeng Wang, "A discretized multi-freedom-degree model for predicting the lowest local resonant gap in phononic structures," Journal of Vibration and Control 20 (11), 1727-1734 (2014).

25 Jin-Chen Hsu. "Local resonances-induced low-frequency band gaps in two-dimensional phononic crystal slabs with periodic stepped resonators."Journal of Physics D: Applied Physics 44.5 (2011): 055401.

26 Larabi, H., et al. "Locally resonant phononic crystals with multilayers cylindrical inclusions." Journal of Physics: Conference Series. Vol. 92. No. 1. IOP Publishing, 2007.

27 Bertoldi K., M. C. Boyce. Wave propagation and instabilities in monolithic and periodically structured elastomeric materials undergoing large deformations [J]. Physical Review B, 2008(78): 184107.

28 Bertoldi K., M. C. Boyce. Mechanically triggered transformations of phononic band gaps in periodic elastomeric structures [J]. Physical Review B, 2008, 7: 052105.

29 Lee, Jae‐Hwang, et al. "25th Anniversary Article: Ordered polymer structures for the engineering of photons and phonons." Advanced Materials 26.4 (2014): 532-569.

30 Yan-Long, Xu, Chang-Qing Chen, and Xiao-Geng Tian. "The existence of simultaneous Bragg and locally resonant band gaps in composite phononic crystal." Chinese Physics Letters 30.4 (2013): 044301.

31 Zhan You Cui, et al. "Experimental and calculated research on a large band gap constituting of tubes with periodic narrow slits." Applied Acoustics 70.8 (2009): 1087-1093.

32 Yongjun Cao, Zhilin Hou, and Youyan Liu. "Convergence problem of plane-wave expansion method for phononic crystals." Physics Letters A, 327.2 (2004): 247-253.

33 A-Li Chen, and Yue-Sheng Wang. "Study on band gaps of elastic waves propagating in one-dimensional disordered phononic crystals." Physica B: Condensed Matter 392.1 (2007): 369-378.

34 Jia-Hong Sun, and Tsung-Tsong Wu. "Propagation of surface acoustic waves through sharply bent two-dimensional phononic crystal waveguides using a finite-difference time-domain method." Physical Review B 74.17 (2006): 174305.

35 Abdelkrim Khelif, et al. "Complete band gaps in two-dimensional phononic crystal slabs." Physical Review E 74.4 (2006): 046610.

36 Yanbo He, Jingtao Du, “Band gap structure analysis of phononic crystal rods with hybrid periodic shunted piezoelectric patches”, Acta Acustica 40(5), 615-624 (2015).

37 Yanbo He, Jingtao Du, “Effects of rotation angle on the band gap structure of two-dimensional phononic crystals with hexagon scantterer,” International conference on vibration and vibro-acoustics, Harbin, Heilongjiang, China, 2014

38 Richard V. Craster, and Sébastien Guenneau, eds. *Acoustic metamaterials: negative refraction, imaging, lensing and cloaking*. Vol. 166. Springer Science & Business Media, 2012.

39 He, Zhaojian, et al. "Extraordinary acoustic reflection enhancement by acoustically transparent thin plates." Applied Physics Letters 100.9 (2012): 091904.

40 D.P. Elford. “Band gap formation in acoustically resonant phononic crystals”, Ph.D thesis, Loughborough University.

41 Pai Wang, et al. "Harnessing buckling to design tunable locally resonant acoustic metamaterials." Physical review letters 113.1 (2014): 014301.

42 Michael Peter Norton, and Denis G. Karczub. *Fundamentals of noise and vibration analysis for engineers*. Cambridge university press, 2003.